REVIEW

ADVANCED
FUNCTIONAL
MATERIALS
www.afm-journal.d

Check for updates

Multiresonant Thermally Activated Delayed Fluorescence Emitters Based on Heteroatom-Doped Nanographenes: Recent Advances and Prospects for Organic Light-Emitting Diodes

Subeesh Madayanad Suresh, David Hall, David Beljonne, Yoann Olivier, and Eli Zysman-Colman*

Since the first report in 2015, multiresonant thermally activated delayed fluorescent (MR-TADF) compounds, a subclass of TADF emitters based on a heteroatom-doped nanographene material, have come to the fore as attractive hosts as well as emitters for organic light-emitting diodes (OLEDs). MR-TADF compounds typically show very narrow-band emission, high photoluminescence quantum yields, and small ΔE_{ST} values, typically around 200 meV, coupled with high chemical and thermal stabilities. These materials properties have translated into some of the best reported deep-blue TADF OLEDs. Here, a detailed review of MR-TADF compounds and their derivatives reported so far is presented. This review comprehensively documents all MR-TADF compounds, with a focus on the synthesis, optoelectronic behavior, and OLED performance. In addition, computational approaches are surveyed to accurately model the excited state properties of these compounds.

1. Introduction

Delayed fluorescence (DF) was first identified by Francis Perin (1929),[1] in uranyl salts. DF was later studied in detail by Magel

Dr. S. Madayanad Suresh, D. Hall, Prof. E. Zysman-Colman
Organic Semiconductor Centre
EaStCHEM School of Chemistry
University of St Andrews
St Andrews KY16 9ST, UK
E-mail: eli.zysman-colman@st-andrews.ac.uk
D. Hall, Prof. D. Beljonne, Prof. Y. Olivier
Laboratory for Chemistry of Novel Materials
University of Mons
Place du Parc 20, Mons 7000, Belgium
Prof. Y. Olivier
Unité de Chimie Physique Théorique et Structurale
and Laboratoire de Physique du Solide
Namur Institute of Structured Matter
Université de Namur
Rue de Bruxelles, 61, Namur 5000, Belgium

The ORCID identification number(s) for the author(s) of this article can be found under https://doi.org/10.1002/adfm.201908677.

and co-workers[2] (1941) in fluorescein followed by studies in other π-conjugated compounds such as eosin,[3] fullerene,[4] benzophenone,[5] aromatic thiones,[6] thioketones,[7] and 9,10-anthraquinone.[8] For many years, molecules for thermally activated delayed fluorescence (TADF), also known as E-type fluorescence for eosin Y, were not given much attention due to the lack of potential applications and the generally low measured photoluminescence quantum yields. In 2009, Adachi and co-workers reported a Sn^{4+} porphyrin as a TADF emitter and employed it in OLEDs.[9] In the following year, Deaton et al. reported a dinuclear copper(I) complexes showing TADF.[10] These initial reports catalyzed a resurgence of interest in the molecular design of copper(I) complexes as emitters for OLEDs by the likes of Yersin and co-workers,[11] Thompson and co-workers,[12] Bräse and co-workers,[13] among many others.[14] The first purely organic TADF emitter used in an OLED was reported by Adachi and co-workers in 2011.[15] The EQE of the OLED was only 5.3%, and thus failed to provide convincing evidence that TADF is activated in the exciton-harvesting process. In 2012, the same group introduced a series of highly efficient organic TADF emitters composed of carbazole electron donating (D) and phthalonitrile accepting (A) units.[16] The resultant structures present a large twisting angle between the D and A units that reduces overlap between the frontier HOMO and LUMO molecular orbitals, and as a result produces a small singlet–triplet energy gap (ΔE_{ST}). The best performing OLED, using the now well-known 4CzIPN, showed an EQE_{max} of 19.3%. This seminal contribution triggered huge research efforts to develop TADF materials for a number of applications[17] aside from electroluminescent devices: these include oxygen sensing,[18] photocatalysis,[19] electrochemiluminescence,[20] lasers,[21] and bioimaging.[22] According to spin statistics, hole and electron recombination upon electrical excitation of the emitter results in a 3:1 ratio of triplet excited states with respect to singlets.[23]

In TADF systems, the lowest excited singlet (S_1) and triplet (T_1) states are very close in energy to each other. The small ΔE_{ST}, typically less than 200 meV, provides an avenue for thermal upconversion of previously nonemissive triplet

**ADVANCED
SCIENCE NEWS**
www.advancedsciencenews.com

**ADVANCED
FUNCTIONAL
MATERIALS**
www.afm-journal.de

excitons into emissive singlet excitons via reverse intersystem crossing (rISC).[17] According to El-Sayed's rule, the two excited states must originate from different orbitals in order to facilitate the required spin–orbit coupling mediating rISC.[24] Via TADF, 100% internal quantum efficiency (IQE) can be realized in EL devices, the result of the harvesting of 100% of the excitons. To achieve high-performance TADF emitters, fast rISC rates are required, which are governed by a combination of small ΔE_{ST} and large spin–orbit coupling (SOC), the latter mediated in part by the presence of heavy atoms in the emitter. Samantha et al. identified that the strength of the SOC in D–A organic molecules relies mainly on difference in the nature of the S_1 and T_1 excited states.[25] However, the emitter must also possess high photoluminescence quantum yield, Φ_{PL}, which is a function of the oscillator strength[26] of the radiative transition from the S_1 state. As a consequence of the D–A molecular design, the lowest singlet and triplet excited states bear a strong intramolecular charge transfer (ICT) character that is linked with a small ΔE_{ST}. However, the small ΔE_{ST} usually is associated with a small oscillator strength of the S_1–S_0 transition as both parameters are essentially proportional to the overlap between the hole and electron densities. It is thus very difficult to obtain TADF emitters that at once present both small ΔE_{ST} and large Φ_{PL}. Another weakness in D–A TADF emitter design is the broad emission band originated from the ICT-emissive singlet state. The broadness both results in poorer color purity and also is emblematic of increased vibrational motion, which can lead to increased nonradiative decay rates.[27]

2. Multiresonant-TADF Emitter Design

Recently, Hatakeyama and co-workers[28] introduced a potential solution, coined multiresonance TADF (MR-TADF), by designing planar boron- and oxygen (or nitrogen)-containing arene compounds. MR-TADF compounds are a new class of fused polycyclic aromatic compounds having electron donating atom (donor) and electron deficient atom (acceptor) disposed *para* to each other in a fused planar polycyclic aromatic framework.[27a,28,29] Due to their complementary resonance effects the electron density distributions on the HOMO and LUMO orbitals are offset by one atom as illustrated in **Figure 1**. In MR-TADF compounds the electron-rich regions are mainly on the donor atoms and carbon atoms positioned *ortho* and *para* to them while the electron-deficient regions are localized on the acceptor atoms and the carbon atoms positioned *ortho* and *para* to them. In the lowest singlet and triplet excited states, the electron density distribution is delocalized over the entire arene but with alternative electron-rich and electron-poor regions while the electron-density distribution shows the same alternating pattern in the ground state, yet with electron-rich and electron-poor regions being switched. The resulting transition from S_1 to S_0 therefore features a short-range reorganization of the electron density while, importantly, maintaining a high degree of electron–hole overlap. In MR-TADF, the Franck–Condon excitations show high oscillator strength, reminiscent of locally excited (LE) states, leading to both efficient delayed fluorescence and high Φ_{PL}. Thus, MR-TADF molecules combine in a rather unique fashion long-range interactions and delocalization

Subeesh Madayanad Suresh obtained his M.Sc. in analytical chemistry from Maharajas College Ernakulum. He then moved to Pusan National University in 2013 for a Ph.D. under the supervision of Prof. Youngson Choe. During this period, his research focused on developing small organic molecules for light-emitting electrochemical cells (LEECs). He then moved to the University of St Andrews for a postdoctoral fellowship with Prof. Eli Zysman-Colman working on the design of thermally activated delayed fluorescent (TADF) emitters for organic light-emitting diodes (OLEDs). In 2019, he received the Marie Skłodowska-Curie Individual Fellowship with Prof. Eli Zysman-Colman for developing MR-TADF emitters for OLEDs and LEECs.

David Hall obtained his MChem from the University of Durham working with Prof. Martin Bryce where he worked on the synthesis of donor–acceptor systems directed toward thermally activated delayed fluorescence (TADF) or room temperature phosphorescence (RTP). Currently, he is a cotutelle student between the University of St Andrews and the University of Mons under the guidance of Prof. Eli Zysman-Colman and Prof. Yoann Olivier, respectively. His research focuses on computational design, synthesis and optoelectronic characterization of novel TADF emitters, primarily multiresonant-TADF compounds.

Eli Zysman-Colman obtained his Ph.D. from McGill University in 2003 with Prof. David N. Harpp as an FCAR scholar. He then completed two postdoctoral fellowships, one Jay Siegel at the University of Zurich as an FQRNT fellow and the other with Stefan Bernhard at Princeton University as a PCCM fellow. He started his independent career in Canada in 2007. In 2013, he moved to the University of St Andrews where he is presently Professor of Optoelectronic Materials and Fellow of the Royal Society of Chemistry. His research program focuses on emitter design for electroluminescent devices and photocatalyst development.
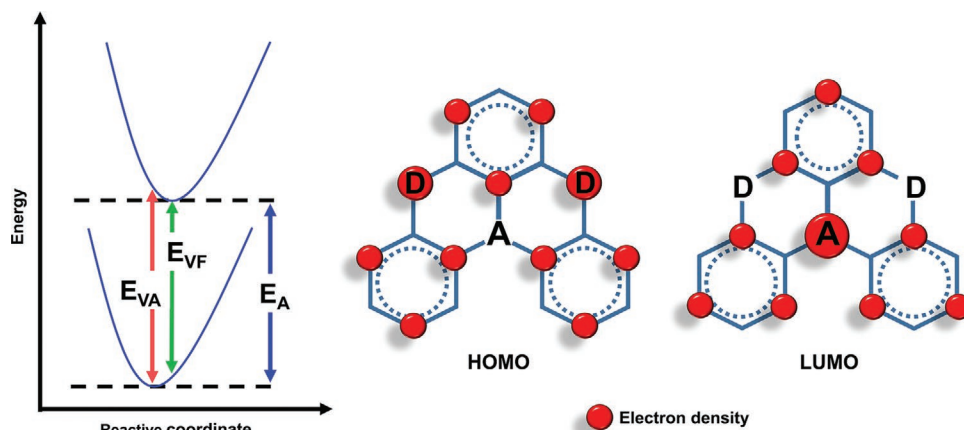
Figure 1. Schematic representation of energy levels and HOMO and LUMO distribution of MR-TADF molecule, where E_{VA} is vertical absorption, E_{VF} is vertical fluorescence, and E_A is adiabatic energy.

effects prompting high radiative decay rates with short-range charge density reshuffling minimizing the singlet–triplet gap. Further, the rigid nature of the emitter results in significantly reduced vibrational motion that is reflected in a much narrower emission band.

In 2015, Hatakeyama and co-workers reported a one-step borylation method to synthesize a series of high band gap B,O-doped polycyclic aromatic molecules with a 1,4-oxaborine substructure.[28] The core structure consists of two donor oxygen atoms and one boron acceptor positioned *para* to both oxygen atoms. The core structure was generated by *ortho* lithiation followed by *trans*-metalation and tandem electrophilic arene borylation of 1,3-diaryloxybenzene and its derivatives. Using these reaction conditions, they synthesized a series of B,O-doped compounds sharing the same 5,9-dioxa-13b-boranaphtho[3,2,1-*de*]anthracene in moderate to good yields (42–74%). The versatility of this one-step borylation is demonstrated by rather diverse examples, including phenyl

and phenoxazine derivatives of B,O core and a boron-fused benzo[6]helicence[28] (**Figure 2**). The electron-rich oxygen atoms accelerate the borylation rate by enhancing the nucleophilicity of the arene. The photophysical properties of the emitters are summarized in **Table 1**. The parent molecule **2a** exhibited near UV emission with a λ_{PL} of 398 nm and high Φ_{PL} of 72% in dichloromethane. The phosphorescence spectrum at 77 K in EtOH glass was observed at 418 nm, which translates to a very high triplet energy level of 2.97 eV. The corresponding ΔE_{ST} for **2a** is small at 0.15 eV, which is comparable to that of a conventional donor–acceptor TADF compounds.[17] Modifying the parent compound with phenyl units (**2b–d**) redshifted the emission maxima to different extents based on the position of phenyl substituents. The most redshifted emission in the series was observed for **2d**, where the both phenyl units are mesomerically conjugated to both oxygen donor atoms; interestingly, no change in the fluorescence maximum, λ_{PL}, was observed when the position of phenyl rings is changed

2a
λ_{PL} 398 nm, τ_{DF} N/A (1 wt% PMMA)
ΔE_{ST} 0.15 eV, Φ_{PL} 72%, FWHM 34 nm (1 wt% PMMA)
λ_{EL} N/A Φ_{EL} N/A, CIE (N/A)
Angew. Chem. Int. Ed., **2015**, 54, 13581

2b
λ_{PL} 410 nm, τ_{DF} N/A (1 wt% PMMA)
ΔE_{ST} 0.21 eV, Φ_{PL} 65%, FWHM 28 nm (1 wt% PMMA)
λ_{EL} N/A Φ_{EL} N/A, CIE (N/A)
Angew. Chem. Int. Ed., **2015**, 54, 13581

2c
λ_{PL} 410 nm, τ_{DF} N/A (1 wt% PMMA)
ΔE_{ST} 0.31 eV, Φ_{PL} 60%, FWHM 33 nm (1 wt% PMMA)
λ_{EL} N/A nm Φ_{EL} N/A, CIE (N/A)
Angew. Chem. Int. Ed., **2015**, 54, 13581

2d
λ_{PL} 436 nm, τ_{DF} N/A ms (1 wt% PMMA)
ΔE_{ST} 0.14 eV, Φ_{PL} 57%, FWHM 49 nm (1 wt% PMMA)
λ_{EL} N/A Φ_{EL} N/A, CIE (N/A)
Angew. Chem. Int. Ed., **2015**, 54, 13581

2e
λ_{PL} 492 nm, τ_{DF} N/A (1 wt% PMMA)
ΔE_{ST} 0.06 eV, Φ_{PL} 92%, FWHM 96 nm (1 wt% PMMA)
λ_{EL} 504 nm Φ_{EL} 13.9, CIE (N/A)
Angew. Chem. Int. Ed., **2015**, 54, 13581

4
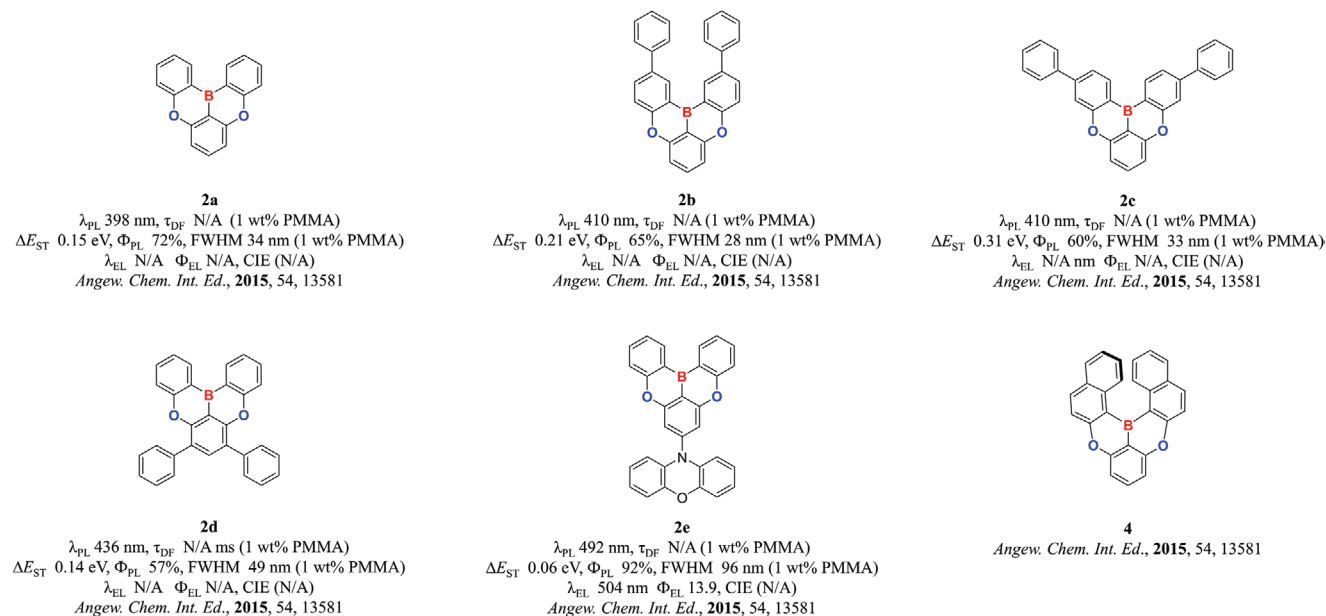*Angew. Chem. Int. Ed.*, **2015**, 54, 13581

Figure 2. Chemical structures, photophysical properties, and device performances of **2a-c** and **4**. Adapted with permission.[28] Copyright 2015, Wiley-VCH.

**ADVANCED
SCIENCE NEWS**
www.advancedsciencenews.com

**ADVANCED
FUNCTIONAL
MATERIALS**
www.afm-journal.de

Table 1. Physical properties of previously reported MR-TADF and those with an MR-TADF acceptor compounds.

Compound	λ_{PL} sol/film [nm][a]	FWHM sol/film [nm][b]	Φ_{PL} sol/film [%][c]	S1 [eV][d]	T1 [eV][e]	ΔE_{ST} [eV][f]	τ_d [g] [μs]	k_{RISC} [h] [s^{-1}]	Ref.
2a	398[i]/N/A	34/–	–/72[j]	3.12[i]	2.97[k]	0.15	–	–	[28]
2b	410[i]/N/A	28/–	–/65[j]	3.02[i]	2.81[k]	0.21	–	–	[28]
2c	410[i]/N/A	33/–	–/60[j]	3.02[i]	2.71[k]	0.31	–	–	[28]
2d	436[i]/N/A	49/–	–/57[j]	2.84[i]	2.70[k]	0.14	–	–	[28]
2e	–/492	–/96	–/92[j]	2.52[j]	2.46[j]	0.06	–	–	[28]
DABNA-1	462[i]/460[l]	33/30	89/88[l]	2.67[l]	2.49[l]	0.18	93.7[l]	9.9×10^{-3l}	[27a]
DABNA-2	470[i]/469[l]	34/28	85/90	2.61[l]	2.47[l]	0.14	65.3[l]	14.8×10^{-3l}	[27a]
2a	403[j]/399[j]	–/26	36/54	3.11[j]	2.90[j]	0.21	–	–	[33]
1	386/–	48/–	63/–	–	–	–	–	–	[35]
B2	461[j]/455[j]	39/32	39/53	2.73[j]	2.54[j]	0.19	–	–	[29a]
B3	442[j]/441[j]	50/34	13/34	2.81[j]	2.66[j]	0.15	–	–	[29a]
B4	449[j]/450[j]	22/38	21/57	2.76[j]	2.61[j]	0.15	–	–	[29a]
B2-F	–/467[j]	–/44	–/57	2.66[j]	2.51[j]	0.15	–	–	[29a]
TBN-TPA	470[m]/–	26[m]/–	97[m]/–	–	–	0.14[m]	51.0[m]	–	[36]
t-DABNA	/445[n]	–/–	–/85[n]	2.80[n]	2.63[n]	0.17	83.3[n]	2.44×10^{3n}	[38]
v-DABNA	468[o]/467[p]	14/18	74/90	2.64[p]	2.62[p]	0.017[p]	4.1[p]	2.0×10^{5p}	[29b]
DOBNA-OAr	388[o]/–	34[o]/–	65[o]/–	–	–	–	–	–	[29b]
TCz-BN[i]	477[m]/–	22[m]/–	–	–	–	–	–	–	[48]
2F-BN	494[m]/502[q]	26/32	95[m]/89[q]	2.51[m]	2.35[m]	0.16	25.9[q]	2.4×10^{4q}	[48]
3F-BN	499[m]/503[q]	27/33	90[m]/83[q]	2.48[m]	2.40[m]	0.08	16.7[q]	3.9×10^{4q}	[48]
4F-BN	496[m]/501[q]	26/31	99[m]/91[q]	2.50[m]	2.39[m]	0.11	19.0[q]	4.4×10^{4q}	[48]
α-3BNOH	390[r]/395[j]	31/32	50/–	3.12[r]	2.81[r]	0.31	0.45[r]	–	[50]
ADBNA-Me-Mes[n]	–/482[p]	–/33	–/89	2.57[p]	2.39[p]	0.18	165.0[p]	7.6×10^{3p}	[54]
ADBNA-Me-Tip[n]	–/479[p]	–/34	–/88	2.59[p]	2.41[p]	0.18	147.0[p]	9.0×10^{3p}	[54]
3[j]	482[j]/485[j]	–	71/84	2.56[j]	2.38[j]	0.18			[55]
4a[j]	485[j]/488[j]	–	88/91	2.54[j]	2.35[j]	0.19			[55]
4b[j]	487[j]/491[j]	–	85/93	2.53[j]	2.34[j]	0.19			[55]
5a[j]	483[j]/485[j]	–	82/91	2.56[j]	2.38[j]	0.18			[55]
5b[j]	486[j]/487[j]	–	81/86	2.55[j]	2.38[j]	0.17			[55]
6a[j]	477, 609[i]/487[j]	–	19/26	2.55[j]	2.38[j]	0.17			[55]
6b[j]	481, 601[i]/495[j]	–	18/24	2.51[j]	2.38[j]	0.13			[55]
m-AC-DBNA	569[i]/492[s]	58/89	–	–	–	0.009[t]	7.6[s]	2.6×10^{5s}	[56]
p-AC-DBNA	557[i]/496[s]	96/96	–	–	–	0.009[t]	1.5[s]	1.2×10^{5s}	[56]
m′-AC-DBNA	568[i]/498[s]	51/87	–	–	–	0.03[t]	7.8[s]	8.4×10^{5s}	[56]
TDBA-Ac	458[u]/	50/–	–/93[v]	3.11[u]	3.05[u]	0.06	1.0[i]	9.9×10^{5v}	[57]
TDBA-DI	456[u]/	55/–	–/99[v]	3.06[u]	2.95[u]	0.11	6.2[i]	10.8×10^{5v}	[57]
OBA-O	444[m]/450[w]	–/80	76/84	3.15[w]	3.06[w]	0.09	4.14	4.3×10^{5w}	[58]
OBA-S	456[m]/470[w]	–/68	63/75	3.17[w]	3.08[w]	0.09	4.80	2.8×10^{5w}	[58]
OBA-BrO	470[m]/476[w]	–/83	84/92	3.25[w]	3.21[w]	0.04	3.74	9.0×10^{5w}	[58]
OBA-BrS	478[m]/470[w]	–/108	53/55	3.19[w]	3.12[w]	0.07	0.81	8.4×10^{5w}	[58]
3CzTB	433[u]/–	–/49	–/88[v]	3.16[u]	2.93[u]	0.23	9.32[v]	1.0×10^{5v}	[59]
M3CzB	445[u]/–	–/42	–/93[v]	3.06[u]	2.92[u]	0.14	7.84[v]	1.4×10^{5v}	[59]
QAO	466[u]/	32/–	–/72[x]	–	–	0.18[u]	93.3[x]	–	[60]
QAO-DAd	548[u]/	49/–	90[y]	–	–	0.01[u]	7.8[y]	–	[60]
3-Ph-QAD	466[u]/478[z]	30/55	–/73[z]	2.60[z]	2.42[z]	0.18	250[z]	1.2×10^{4z}	[62]

**ADVANCED
SCIENCE NEWS**

www.advancedsciencenews.com

**ADVANCED
FUNCTIONAL
MATERIALS**

www.afm-journal.de

Table 1. Continued.

Compound	λ_{PL}sol/film [nm][a]	FWHMsol/film [nm][b]	Φ_{PL} sol/film [%][c]	S1 [eV][d]	T1 [eV][e]	ΔE_{ST} [eV][f]	τ_d[g] [μs]	k_{RISC}[h] [s^{-1}]	Ref.
7-Ph-QAD	464[u]/472[z]	22/58	–/68[z]	2.63[z]	2.44[z]	0.19	474[z]	6.4×10^{3z}	[62]
DiKTa	453[u]/463[z1]	27/37	26/75	2.75[z1]	2.55[z1]	0.20	15[z1]	4.6×10^{4u}	[63]
Mes₃DiKTa	468[u]/477[z1]	29/37	37/80	2.67[z1]	2.46[z1]	0.21	20[z1]	3.1×10^{4u}	[63]

[a]Photoluminescence emission maxima; [b]Full width half-maxima from the PL spectrum; [c]Absolute photoluminescence quantum yield; [d]Estimated energy level of the S_1 state from fluorescence maximum at 77 K; [e]Estimated energy level of the T_1 state from phosphorescence maximum at 77 K; [f]Energy difference between singlet and triplet excited states determined from fluorescence and phosphorescence emission maxima at 77 K; [g]Lifetimes calculated from the fluorescence decay; [h]Reverse intersystem crossing decay rate from T_1 to S_1; [i]Obtained in CH_2Cl_2 solution; [j]Obtained in 1 wt% emitter in PMMA; [k]Obtained in EtOH (saturated); [l]Obtained in 1 wt% mCBP; [m]Obtained in toluene 10^{-5} M; [n]Doped in DPEPO; [o]Obtained in 0.02×10^{-3} M in toluene; [p]Obtained in 1 wt% DOBNA-OAr; [q]Obtained in 6 wt% doped in mCPBC; [r]Obtained in 10^{-5} M THF; [s]Obtained in 5 wt% doped in BCPO; [t]Determined from the Arrhenius plot for k_{RISC}; [u]Obtained in 10^{-5} M toluene; [v]Obtained from 20 wt% doped in DBFPO; [w]Obtained in 10 wt% doped in mCP; [x]Obtained in 10 wt% doped in mCP; [y]Obtained in 5 wt% CBP; [z]Obtained in 2 wt% doped in mCP; [z1]Obtained in 3.5 wt% doped in mCP.

from *para* to the donor oxygen atoms (**2b**) to *meta* to the donor oxygen in **2c**. However, this shift of phenyl substitution pattern significantly redshifted the phosphorescence maxima, and in the case of **2c**, resulted in a large ΔE_{ST} (0.31 eV) compared to **2b** (0.21 eV). Finally, this multiresonant core was connected to a strong electron-donating phenoxazine unit to generate **2e**, that behaved as a typical D–A TADF molecule. It is not surprising that **2e** showed the largest full width at half-maximum (FWHM = 96 nm) and redshift of emission (λ_{PL} = 492 nm) compared to the parent molecule, **2a** (λ_{PL} = 398 nm, FWHM = 34 nm) in DCM. Surprisingly, given a ΔE_{ST} of only 0.06 eV, the Φ_{PL} is very high at 92% and the combination of these two properties was noted to be extremely beneficial to have in a TADF emitter.[30] In the same report, the authors synthesized a boron-fused benzo[6]helicene (**4**) from 1,3-bis(naphthalen-2-yloxy)benzene in 33%. Notably, the unsymmetrical isomer was formed only in 2% yield (not isolated). The photophysical characterization was unfortunately not provided in the original report.

The potential of these high triplet energy compounds as host materials in vacuum-deposited OLEDs was demonstrated using a well-known phosphorescent green emitter *fac*-Ir(ppy)₃, with performance compared to that of a device using the widely used host (CBP).[28] Device performances are given in **Table 2**. Fused planar ring compounds are known to show aggregation in the solid state. In the case of **2a** and **2b**, these tended to crystallize rapidly in thin film, which ruled them out as host materials. It is somewhat surprising that **2b** showed tendency to crystalize, but this was not the case with **2c** and **2d**. The fabricated devices with **2c** and **2d** acting as hosts outperformed the devices using CBP in terms of driving voltage, current efficiency, power efficiency and external quantum efficiency, and more importantly, the device lifetime.[28] For the device stack ITO (100 nm)/ dipyrazino[2,3-f:2′,3′-h]quinoxaline-2,3,6,7,10,11-hexacarbonitrile (HAT-CN) (10 nm)/$N^4,N^4,N^{4'},N^{4'}$-tetra([1,1′-biphenyl]-4-yl)-[1,1′-biphenyl]-4,4′-diamine (TBBD) (60 nm)/tris(4-carbazolyl-9-ylphenyl)amine (TCTA) (10 nm)/5 wt% *fac*-Ir(ppy)₃ in **2c** or **2d** (30 nm)/1,3,5-tris(1-phenyl-1*H*-benzo[d]imidazol-2-yl)benzene) (TPBi) (50 nm)/LiF (1 nm)/Al (100 nm), the lifetimes, LT_{80} (LT_{80} = the time for the luminance to decay to 80% of the initial luminance, defined in this case as 2000 cd m⁻²) for OLEDs employing **2c** and **2d** were 1000 and 383 h, respectively, while LT_{80} for the OLED using CBP in the device configuration ITO/HAT-CN/TCTA/5 wt% *fac*-Ir(ppy)₃ in CBP/TPBi/LiF/Al

was only 95 h. The hosts **2c** and **2d** outperformed CBP in terms of current efficiency (η_c), power efficiency (η_p) and external quantum efficiency at 1000 cd m⁻² (EQE_{1000}). The EQEs at 1000 cd m⁻² were 20.1%, 20.6%, and 17.6% for devices based on **2c**, **2d**, and CBP, respectively. The corresponding η_c and η_p values at 1000 cd m⁻² were 72.1 cd A⁻¹ and 43.5 lm W⁻¹ for **2c**, 73.8 cd A⁻¹ and 41.9 lm W⁻¹ for **2d**, and finally, 63.3 cd A⁻¹ and 34.1 lm W⁻¹ for devices based on CBP. Surprisingly, when **2e** was the emitter and using a similar device stack architecture with the primary difference being the use of 20 wt% doping of the emitter, the LT_{80} was poor at less than 1 h, regardless of choice of host material: **2c** or CBP. However, **2c** worked better than CBP in this case too. The EQE_{1000} for these devices with **2c** and CBP as hosts were 15.2% and 13.9%, respectively. The current and power efficiency were noted to be 52.8 cd A⁻¹ and 36.0 lm W⁻¹ for devices with **2c** as host at 1000 cd m⁻².

In 2016, Hatakeyama et al. introduced related MR-TADF compounds, replacing the oxygen donor atoms for tricoordinate nitrogen atoms.[27a] The use of the more Lewis basic nitrogen atom donors produced a desired redshift of the emission in this new series of compounds. Emission remained narrow and ΔE_{ST} remained small, thus conserving the TADF character of these nitrogen-containing emitters. Typically, color filters and/or an optical micro cavity are used in order to improve color purity in commercial displays to compensate for the broad emission profile. It is therefore not surprising that these narrow-band emitters have attracted much attention in OLED research as these optical compensation tools would no longer be needed. More importantly, with this evolved design strategy a family of deep blue emitters now became accessible. The molecular structure consists of a triphenylborane core and incorporating two nitrogen atoms that are each phenyl substituted *para* to the central boron atom (**Figure 3**). The initial report contained two structurally related emitters, **DABNA-1** and **DABNA-2**, where the primary difference between the two is an appended diphenyl amine group and two phenyl substituents. Just like its oxygen-containing analogs, the opposing resonance effects of nitrogen donor and boron acceptor atoms separate HOMO and LUMO electron density distributions, leading to small ΔE_{ST} and large oscillation strength for the $S_1–S_0$ transition. The synthesis of these two compounds relied on the same boron cyclization protocol previously employed (insertion of boron and cyclization),[28]

Table 2. Best device performances of previously reported MR-TADF and those with an MR-TADF acceptor compounds.

Compound	λ_{EL} [nm][a]	FWHM [nm][b]	CIE (x, y)[c]	Brightness_Max/[cd m^{-2}][d]	CE_MAX/CE_100/ CE_1000 [cd A^{-1}][e]	PE_MAX/PE_100/ PE_1000 [lm W^{-1}][f]	EQE_MAX/EQE_100/ EQE_1000 [%][g]	Efficiency Roll-off [%][h]	Ref.
2e[i]	504	–	–	–	–/–/52.8	–/–/36.0	–/–/15.2	–	[28]
DABNA-1[j]	459	28	0.13, 0.09	<1000	10.6/–/–	8.3/–/–	13.5/6.3/–	53	[27a]
DABNA-2[j]	467	28	0.12, 0.13	<1000	21.1/14.2/–	15.1/7.9/–	20.2/13.4/–	34	[27a]
B2[j]	460	37	0.13, 0.11	<1000	16.7/11.5/–	13.8/7.1/	18.3/12.6/–	31	[29a]
TBN-TPA[k]	474	27	0.13, 0.19	16 593	40.2/34.4/17.4	30.0/23.5/8.8	32.1/27.4/13.9	15	[36]
t-DABNA[l]	466	31	0.13,0.15	–	32.6/28.9/20.9	33.6/21.0/10.9	31.4/27.2/19.8	13	[38]
v-DABNA[m]	469	18	0.12, 0.11	–	31.0/29.5/23.2	25.6/20.8/23.2	34.4/32.8/26.0	5	[29b]
TCz-BN[n]	474	34	0.13, 0.20	–	–	24/17.0/10.0	18.9/15.2/10.5	20	[48]
2F-BN[n]	501	40	0.16, 0.60	–	–	69.8/60.1/38.1	22.0/20.1/15.0	9	[48]
3F-BN[n]	499	39	0.20, 0.58	–	–	72.3/63.1/45.9	22.7/22.3/21.1	2	[48]
4F-BN[n]	493	32	0.12, 0.48	–	–	51.3/42.4/29.4	20.9/19.2/16.4	8	[48]
ADBNA-Me-Mes[o]	481	32	0.10, 0.27	<1000	25.5/16.6/–	19.3/10.0/–	16.2/11.1/–	31	[54]
ADBNA-Me-Tip[o]	480	33	0.11, 0.29	<1000	34.7/23.5/–	28.7/14.9/–	21.4/15.4/–	28	[54]
m-AC-DBNA[p]	492	–	0.18, 0.42	24 600	42.0/39.1/32.0	34.1/22.3/13.4	17.1/16.0/13.2	6	[56]
p-AC-DBNA[p][q]	500	–	0.23, 0.49	69 160	54.4/54.4/5.07	49.8/42.8/28.9	19.2/19.1/18.2	1	[56]
m'-AC-DBNA[p]	492	–	0.18, 0.29	21 160	35.3/28.8/24.1	29.3/16.5/10.1	14.1/12.0/10.2	15	[56]
TDBA-Ac[r]	468	55	0.14, 0.15	9014	27.7/–/20.4	25.4/–/10.9	25.7/–/18.9	–	[57]
TDBA-DI[r]	481	65	0.15, 0.28	47 680	64.4/–/57.0	57.2/–/33.0	38.2/–/34.3	–	[57]
OBA-O[s]	446	–	0.17, 0.17	6785	33.2/28.3/16.3	34.2/26.5/11.7	17.8/15.5/8.5	13	[58]
OBA-S[s]	488	–	0.20, 0.31	3583	6.3/1.7/1.0	5.8/1.2/0.3	4.4/1.3/0.7	70	[58]
OBA-BrO[s]	500	–	0.21, 0.38	1695	49.2/26/7.1	56.9/22.5/4.3	22.5/12.5/3.1	44	[58]
OBA-BrS[s]	520	–	0.29, 0.46	959	20.3/1.7/–	20.9/0.9/–	9.2/0.8/–	91	[58]
3CzTB[t]	470	–	0.14,0.19	11 690	36.4/–/17.1	–	29.1/21/13.5	28	[59]
M3CzB[t]	478	–	0.14,0.26	18 160	46.7/–/31.4	–	30.7/28/21.6	9	[59]
QAO[u]	468	39	0.13, 0.18	<1000	26.2/	31.6/	19.4/9.2/–	53	[60]
QAO-DAd[v]	552	–	0.41, 0.56	<10 000	83.3/–/–	75.0/–/–	23.9/22.8/–	5	[60]
3-Ph-QAD[w]	480	44	0.13, 0.32	4975	33.5/19.3/–	32.9/16.0/–	19.1/11/–	42	[62]
7-Ph-QAD[w]	472	34	0.12, 0.24	2944	28.8/8.8/–	28.2/8.8/–	18.7/5.8/–	69	[62]
DiKTa[x]	465	39	0.14, 0.18	10 385	–	–	14.7/8.3/3.3	44	[63]
Mes₃DiKTa[x]	480	36	0.12, 0.32	12 949	–	–	21.1/14.5/4.5	31	[63]

[a]Electroluminescence emission maxima; [b]Full width at half-maxima of the EL spectrum; [c]Commission Internationale de l'Eclairage coordinates from the EL spectrum; [d]Maximum brightness achieved with the device; [e]Current efficiency; [f]Power efficiency; [g]External quantum efficiency; [h]Obtained using the equation (($EQE_{max} - EQE_{100}$)/EQE_{MAX}) × 100; [i]ITO/HAT-CN/TCTA/20 wt% **2e** in **2c**/TPBi/LiF/Al; [j]ITO (50 nm); NPD (40 nm); TCTA (15 nm); mCP (15 nm); 1 wt% emitter; mCBP (20 nm); TSPO1 (40 nm); LiF (1 nm); and Al (100 nm); [k]ITO/MoO3 (2.5 nm)/TAPC (30 nm)/2,6-DCzppy: 4 wt% TBN-TPA (10 nm)/TmPyPB (30 nm)/LiF(1 nm)/Al (100 nm); [l]PEDOT:PSS(60 nm)/TAPC; (20 nm)/mCP; (10 nm)/5 wt% emitter DPEPO:DMAC-DPS (25 nm)/TSPO1; (5 nm)/TPBi; (20 nm)/LiF (1.5 nm)/Al (200 nm); [m]ITO, 50 nm; NPD, 40 nm; TCTA, 15 nm; mCP, 15 nm; 1 wt% v-DABNA emitter and 99 wt% DOBNA-OAr (20 nm); TSPO1, 30 nm; LiF (1 nm); Al (100 nm); [n]ITO/HAT-CN (10 nm)/NPB (30 nm)/BCzPh (10 nm)/EML(20 nm)/9Cz46Pm (10 nm)/DPPyA:Liq(1:1, 30 nm)/LiF (0.5 nm)/Al (150 nm); [o]ITO (50 nm), HAT-CN hexacarbonitrile (5 nm), NPD (35 nm), TCTA (15 nm), mCP (15 nm), 1 wt% ADBNA emitter and 99 wt% DOBNA-OAr (20 nm), TSPO1 (40 nm), LiF (1 nm), and Al (100 nm); [p]ITO/HATCN (4.2 nm)/TAPC (34 nm)/10 wt% emitter in BCPO (23 nm)/TmPyPB (21 nm)/LiF(1 nm)/Al (100 nm); [q]35% emitter in BCPO used for EML; [r]ITO/HATCN (7 nm)/TAPC (50 nm)/DCDPA (10 nm)/DBFPO 20% emitter (25 nm)/DBFPO (10 nm)/TPBi (20 nm)/LiF (1.5 nm)/Al (100 nm); [s]ITO/HATCN (5 nm)/TAPC(40 nm)/5 wt% emitter: mCP (20 nm)/TmPyPB (40 nm)/LiF (1 nm)/Al (100 nm); [t]ITO (50 nm)/TAPC (50 nm)/DCDPA (10 nm)/DBFPO:20 wt% dopant (25 nm)/DBFPO (5 nm)/TPBi (15 nm)/LiF/Al (1.5/100 nm); [u]ITO/HATCN, 10 nm)/TAPC, (45 nm)/TCTA, (10 nm)/5 wt% QAO:mCP (20 nm)/B3PYMPM (40 nm)/Liq, (2 nm)/Al (120 nm); [v]ITO/HATCN(10 nm)/TAPC (45 nm)/TCTA (10 nm)/5 wt% QAO-DAd:CBP(20 nm)/1,3,5-tri(m-pyrid-3-yl-phenyl)benzene (TmPyPB, 50 nm)/Liq (2 nm)/Al (120 nm); [w]ITO/TAPC (35 nm)/TCTA (10 nm)/mCP: 2 wt% dopant (20 nm)/TmPyPB (40 nm)/LiF (1 nm)/Al; [x]ITO/HAT-CN (10 nm)/TAPC (40 nm)/TCTA (10 nm)/3.5 wt% emitter:mCP (20 nm)/TmPyPb (50 nm)/LiF (1 nm)/Al (100 nm).

starting with a lithium-chloride exchange reaction followed by trans-metalation to boron and then electrophilic arene borylation **Scheme 1**. **DABNA-1** was synthesized in two steps from a commercially available starting material in 21% overall yield while for **DABNA-2**, the synthesis involved three steps and the product was obtained in 22% overall yield. The robustness and scalability of the synthetic protocol was demonstrated by carrying out gram-scale reactions.

In dilute CH_2Cl_2 solutions both emitters exhibited narrow emission with λ_{PL} of 462 and 470 nm, respectively, for **DABNA-1**
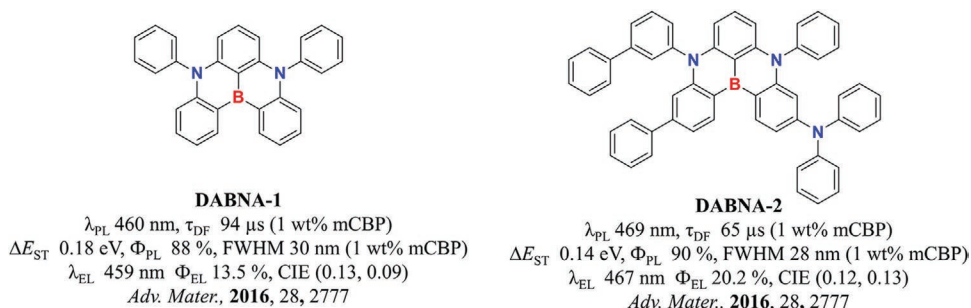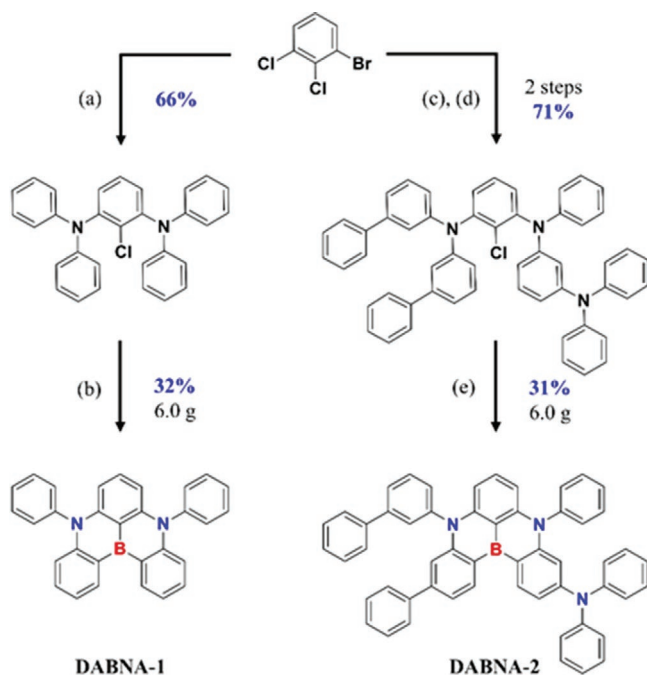
DABNA-1
λ_{PL} 460 nm, τ_{DF} 94 μs (1 wt% mCBP)
ΔE_{ST} 0.18 eV, Φ_{PL} 88 %, FWHM 30 nm (1 wt% mCBP)
λ_{EL} 459 nm Φ_{EL} 13.5 %, CIE (0.13, 0.09)
Adv. Mater., **2016**, 28, 2777

DABNA-2
λ_{PL} 469 nm, τ_{DF} 65 μs (1 wt% mCBP)
ΔE_{ST} 0.14 eV, Φ_{PL} 90 %, FWHM 28 nm (1 wt% mCBP)
λ_{EL} 467 nm Φ_{EL} 20.2 %, CIE (0.12, 0.13)
Adv. Mater., **2016**, 28, 2777

Figure 3. Chemical structures, photophysical properties, and device performances of **DABNA-1** and **DABNA-2**. Adapted with permission.[27a] Copyright 2016, Wiley-VCH.

and **DABNA-2** and very small FWHM of ≈33 nm. Unlike typical charge transfer D–A TADF emitters, **DABNA-1** and **DABNA-2** show essentially no positive solvatochromism. In fact, the emission from CH_2Cl_2 to EtOH is blueshifted by 4 and 7 nm, respectively, for **DABNA-1** and **DABNA-2**, which clearly indicates the nonpolar character of the lowest singlet excitations. In 1 wt% mCBP the Φ_{PL} values of these emitters remain very high at 88% and 90%, respectively, for **DABNA-1** and **DABNA-2**. ΔE_{ST} and k_{RISC} for **DABNA-1** and **DABNA-2** were calculated to be 0.18 eV and 9.9×10^3 s^{-1}, 0.14 eV, and 14.8×10^3 s^{-1}, respectively. The presence of the substituents in **DABNA-2** improves the molar excitation coefficient, ε, in the absorption spectrum and also

the Φ_{PL} of the emitter. However, the presence of these substituents caused an undesired redshift in the emission. The delayed fluorescence lifetimes, τ_d, were 93.7 and 65.3 μs **DABNA-1** and **DABNA-2**, respectively, in 1 wt% 3,3′-bis(N-carbazolyl)-1,1′-biphenyl (mCBP) films at 300 K.

Finally, the potential of both the emitters in OLEDs were assessed in the device stack ITO (50 nm); N,N′-di(1-naphthyl)-N,N′-diphenyl-(1,1′-biphenyl)-4,4′-diamine (NPD) (40 nm); TCTA (15 nm); 1,3-bis(N-carbazolyl)benzene (mCP) (15 nm); 1 wt% **DABNA-1** or **DABNA-2** emitter; mCBP (20 nm); diphenyl-4-triphenylsilylphenylphosphine oxide (TSPO1) (40 nm); LiF (1 nm); and Al (100 nm). As expected from the photoluminescence emission measurements, **DABNA-1** exhibited an emission centered at λ_{EL} of 459 nm with an impressively small FWHM of 28 nm. Notably, these chromaticity values are of commercial relevance for displays where the CIE coordinates presented by this device (0.13, 0.09) were noted to be close to that of the National Television System Committee (NTSC) standard of (0.14, 0.08). The emission color was identified as good as that of the best values reported for fluorescent blue emitters[31] and even comparable to that of a blue emission from a color filter-assisted Samsung galaxy S5 smart phone OLED display (FWHM = 23 nm) measured for the purpose of comparison in their report. The maximum EQE, current and power efficiencies observed for the **DABNA-1** device were 13.5%, 10.6 cd A^{-1}, and 8.3 lm W^{-1}, respectively, at 0.6 cd m^{-2}. Unfortunately, this device showed a significant efficiency roll-off at high current densities. The OLED performance with **DABNA-2** was impressive with an EQE$_{max}$, current and power efficiencies of 20.2%, 21.1 cd A^{-1}, and 15.1 lm W^{-1}, respectively, at 3.2 cd m^{-2}; similar to the **DABNA-1** device, efficiency roll-off was severe with EQE$_{100}$ of 13.4% at 100 cd m^{-2} with corresponding current and power efficiencies values of 14.2 cd A^{-1} and 7.9 lm A^{-1}. The maximum IQE of the OLED with **DABNA-2** was determined to be nearly 100%, which indicates the success of the design strategy and the high TADF efficiency in the device compare to its parent core. Compared to the OLED with **DABNA-1** the device with **DABNA-2** exhibited a slight redshift of the EL spectrum (λ_{EL} = 467 nm, CIE = 0.12, 0.13); however, the FWHM remained very narrow (28 nm) as was the case for its PL spectrum. The authors also fabricated **DABNA-2** devices with a higher doping concentration of emitter from 1 to 5 wt%, which showed a slight increase in device performance coupled with a redshift in the emission [λ_{EL} = 471 nm, CIE = (0.12, 0.17)]. The EQE$_{max}$, current efficiency, and power efficiencies are 20.0%, 23.8 cd A^{-1},

Scheme 1. Synthesis of **DABNA-1** and **DABNA-2**. a) HNPh$_2$ (2.2 equiv.), t -BuOK (2.5 equiv.), (AMPHOS)$_2$PdCl$_2$ (1.0 mol%), o-xylene, 80 °C, 2 h then 120 °C, 3 h. b) t-BuLi (1.2 equiv.), t-butylbenzene, 60 °C, 2 h; BBr$_3$ (1.2 equiv.), rt, 0.5 h; EtN(i-Pr)$_2$ (2.0 equiv.), 120 °C, 3 h. c) HNPh(m-Ph$_2$N-C$_6$H$_4$) (1.0 equiv.), t-BuOK (1.5 equiv.), (AMPHOS)$_2$ PdCl$_2$ (0.5 mol%), o-xylene, 90 °C, 2.5 h. d) HN(m-Ph-C$_6$H$_4$)$_2$ (1.0 equiv.), t-BuOK (1.5 equiv.), (AMPHOS)$_2$PdCl$_2$ (1.0 mol%), o-xylene, 120 °C, 1 h. e) t-BuLi (2.0 equiv.), t-butylbenzene, 60 °C, 3 h; BBr$_3$ (2.0 equiv.), rt, 0.5 h; EtN(i-Pr)$_2$ (2.0 equiv.), 120 °C, 1.5 h. AMPHOS: di-*tert*butyl(p-dimethylaminophenyl)phosphine. Adapted with permission.[27a] Copyright 2016, Wiley-VCH.

and 17.0 lm W^{-1} at 4.1 cd m^{-2} and of 14.8%, 18.0 cd A^{-1}, and 10.1 lm W^{-1} at 100 cd m^{-2}, respectively. **DABNA-1** and **DABNA-2** were also investigated as organic semiconductor laser materials in another report[21] and these multiresonant emitters achieved light amplification better than phosphorescent or even conventional D–A TADF systems.[32] **DABNA-2** presented a large stimulated emission cross-section and also a favorable window for light amplification. A codeposited film of 6 wt% of **DABNA-2** in mCBP showed a nonlinear increase of emission intensity and a decrease of emission band width with increase in excitation intensity due to light amplification.

Following their pioneering DABNA series, the same group prepared a deep-blue-emitting boron-centered 4,8,12-triazatriangulene (also denoted as **2a**; **Figure 4**).[33] The versatility of the synthesis of these triazatriangulene compounds is demonstrated by the synthesis of related boron-, phosphorus-, and silicon-centered derivatives. The boron-centered triangulene **2a** (Figure 4) was synthesized in five steps again employing the same key boron insertion and cyclization steps in a one pot cascade reaction[27a,28,34] in 11% overall yield. Compound **2a** (Figure 4) exhibited excellent thermal and chemical stability toward, oxygen, 1 N HCl, and 1 N NaOH. The planar nature of **2a** (Figure 4) was revealed by single crystal X-ray diffraction analysis (total C−B−C bond angle = 359.9°). In addition, the B−C bonds in **2a** (1.478(7)–1.480(11) Å) are much shorter than typical triaryl boranes such as Ph$_3$B (1.571–1.589 Å). The emission spectrum of **2a** (Figure 4) in a 1 wt% PMMA film showed a narrow emission band at 399 nm (Φ_{PL} = 54%) with a remarkably high triplet energy (E_T = 2.90 eV) and a small ΔE_{ST} of 0.21 eV. As with the DABNA series, the FWHM for this emission was only 26 nm, which was attributed to the rigid, fused structure. Notably, the increase in the number of donor nitrogen atoms surrounding the central boron does not redshift the emission spectrum of **2a** (Figure 4) as compared to **DABNA-1** (λ_{PL} = 460 nm in 1 wt% mCP). Quite the contrary, the λ_{PL} of **2a** (Figure 4) was significantly blueshifted. In classical TADF compounds, the number of donors and acceptors has a significant influence on both the energies of S$_1$ and ΔE_{ST}, while in MR-TADF compounds, this is not the case. When the boron atom is replaced by phosphorus (**2b**) or silicon (**2c**), the resulting compounds lose their planarity and thus emission becomes weak. Both **2b** and **2c** adopt a bowl-shaped structure in the packed crystal. No devices were fabricated with any of the compound in this report to understand their potential as OLED materials.

An oxygen analog of **2a** (Figure 4) was reported by Oi and co-workers in 2016.[35] Compound **1** was obtained following a five-step reaction sequence. Insertion of boron and subsequent cyclization was conducted in one-pot synthesis, which proceeds in 22% isolated yield. The structure of **1** (Figure 4) closely resembles that of **2a** (Figure 4) with a total O−B−C bond angle of 360° and very short C−B bond lengths (1.459–1.461 Å). Further, their photophysics is remarkably similar to **1** (Figure 4) showing deep-blue emission (λ_{PL} = 386 nm, Φ_{PL} = 63, toluene), high triplet energy (λ_{Phos} = 400–414 nm), as well as high chemical and thermal stabilities. Surprisingly, however, no delayed emission was observed in the time-resolved PL spectrum. Further, the emission spectrum of **1** (Figure 4) was significantly broader (FWHM = 48 nm) and showed a larger Stokes shift (47 nm); no devices were fabricated in this report.

In 2018, Hatakeyama's group introduced a simplified borylation reaction by demonstrating selective double and triple borylation of triarylamine via intra- and intermolecular bora Friedel Crafts-type reactions (**Scheme 2**).[29a] This reaction protocol enabled the conversion of 11 C−H bonds to C−B bonds in one shot, a feat that was impossible to achieve using their previously reported methodology. The compound **B2** (**Figure 5**) was prepared in 76% isolated yield by refluxing triarylamine in the presence of 5.0 equivalents of BI$_3$ and 2.0 equivalents of Ph$_3$B. When the bath temperature was raised to 200 °C, triple borylation took place to afford **B3** in 45% isolated yield; it was noted that the use of other boron sources such as BBr$_3$ and BCl$_3$ did not produce any of the desired compounds. In addition, the key role of Ph$_3$B in generating **B3** was demonstrated by carrying out reactions with other commonly used Brønsted bases such as EtN^{i}Pr$_2$ and N,N-dimethyltoluidine. During the reaction screening, target **B3** was only formed in the presence of Ph$_3$B. Even in the presence of same amount of Mes$_3$B, yields of the products were poorer than that of reactions using Ph$_3$B. The authors proposed that Ph$_3$B suppresses side reactions by removing HI from the reaction mixture, which thereby inhibits the undesired retro-Friedel–Crafts reaction. Just like other structurally constrained boron-containing aromatic fused ring compounds, **B2–B4** showed enhanced chemical and thermal stability. Using the same synthetic protocol, the authors were successful in borylating an electron-deficient fluorine-substituted
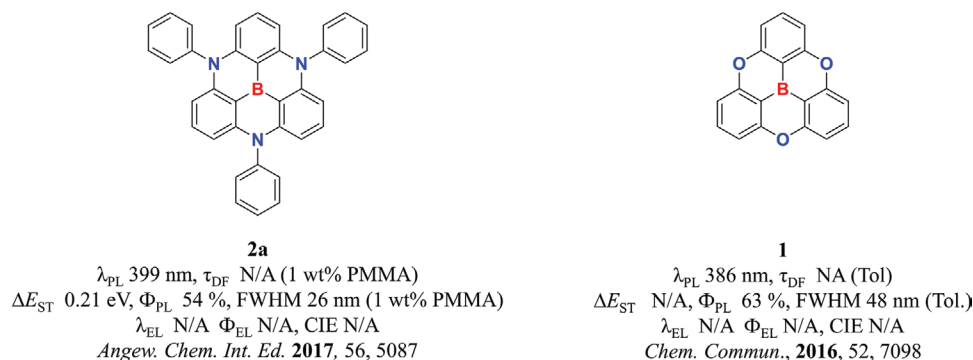

2a
λ_{PL} 399 nm, τ_{DF} N/A (1 wt% PMMA)
ΔE_{ST} 0.21 eV, Φ_{PL} 54 %, FWHM 26 nm (1 wt% PMMA)
λ_{EL} N/A Φ_{EL} N/A, CIE N/A
Angew. Chem. Int. Ed. **2017**, 56, 5087

1
λ_{PL} 386 nm, τ_{DF} NA (Tol)
ΔE_{ST} N/A, Φ_{PL} 63 %, FWHM 48 nm (Tol.)
λ_{EL} N/A Φ_{EL} N/A, CIE N/A
Chem. Commun., **2016**, 52, 7098

Figure 4. Chemical structures and photophysical properties of **2a** (Adapted with permission.[33] Copyright 2017, Wiley-VCH) and **1** (Adapted with permission.[35] Copyright 2016, Royal Society of Chemistry).
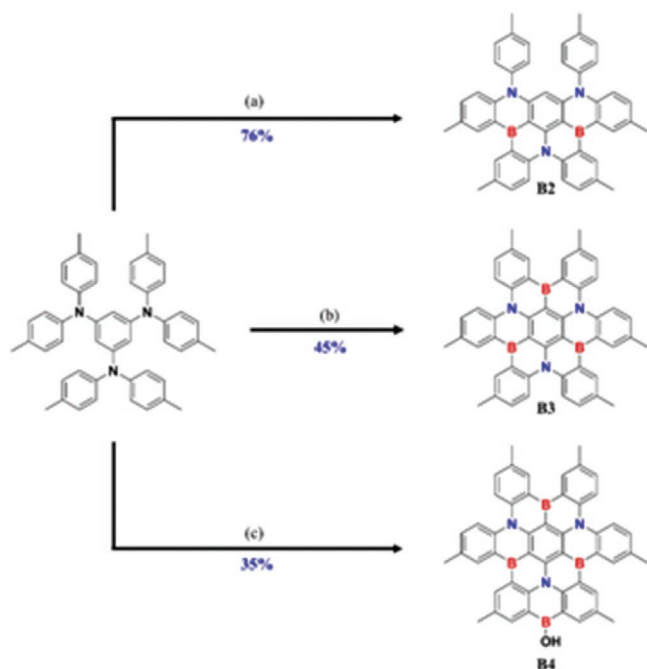
Scheme 2. a) BI_3 (5.0 equiv.), Ph_3B (2.0 equiv.), 1,2-dichlorobenzene, 190 °C, 20 h, b) BI_3 (5.0 equiv.), Ph_3B (2.0 equiv.), 1,2,4-trichlorobenzene, 200 °C, 20 h, and c) BI_3 (12.0 equiv.), Ph_3B (2.0 equiv.), 1,2-dichlorobenzene, 200 °C, 12 h. Adapted with permission.[29a] Copyright 2018, American Chemical Society.

substrate (**B2-F**; **Figure 6**). Double borylation of the substrate took place at 200 °C in good yields (58%); however, it was not possible to triply or quadruply borylate the substrate, even at 240 °C. Single crystal X-ray diffraction analysis reveals that **B3** has a triple helical structure. Due to a large difference between the C−B and C−N bond lengths and the methyl substituents, **B3** exhibited D_3 symmetry, which is in contrast to the all carbon analog (hexabenzo[a,d,g,j,m,p]coronene that presents D_{3d} symmetry).[29a] The dihedral angle between peripheral benzene rings (30.3°–48.2°) exhibited a wider range when compared to

the all carbon analog (43°–45°). Nucleus-independent chemical shifts (NICS) values indicate that the central benzene in **B3** has similar aromatic character to the central benzene in hexabenzo[a,d,g,j,m,p]coronene, while all the neighboring six rings have antiaromatic character.

The photophysical properties of **B2-B4** were investigated in 1 wt% PMMA. The absorption maximum of the lowest energy band of **B3** (λ_{abs} = 396 nm) is significantly blueshifted from those of **B2** (λ_{abs} = 438 nm), **B2-F** (λ_{ab} = 437 nm) and **B4** (λ_{ab} = 440 nm). From the reported time-dependent density functional theory (TD-DFT) calculations, this band was identified as originating from S_0–S_3 and S_0–S_4 transitions, which are degenerate and spin-allowed (f = 0.5200), while the lower-energy S_0–S_1 and S_0–S_2 transitions are very weak (f = 0.0006). All the emitters exhibited narrow blue emission at λ_{PL} of 455, 467, 441, and 450 nm, respectively, for **B2**, **B2-F**, **B3**, and **B4**. The emitter **B2** exhibited the smallest FWHM of 32 nm (λ_{PL} = 455 nm); when this structure is functionalized with fluorine atoms, **B2-F**, the emission broadens (FWHM = 44 nm) and redshifted by 17 nm. The emission of **B3** is the bluest in the series, but unfortunately also possesses the lowest Φ_{PL} of 33%. The ΔE_{ST} values, determined from the energy difference between the room temperature fluorescence and 77 K phosphorescence spectra, are all sufficiently small (ΔE_{ST} ranging from 0.15 to 0.19 eV) to promote rISC. Notably, the PL spectra of **B2** and **B3** exhibited CIE coordinates of (0.14, 0.08) and (0.15, 0.06), respectively, which satisfy the requirements for blue emission defined by NTSC (0.14, 0.08) and the European Broadcasting Union, EBU (0.15, 0.06).

The potential of these blue TADF emitters in EL devices was demonstrated by applying **B2** as the emitter in the OLED stack ITO (50 nm); NPD (40 nm); TCTA (15 nm); mCP (15 nm); 1 wt% **B2** in mCBP (20 nm); TSPO1 (40 nm); LiF (1 nm); Al (100 nm). As expected from the PL measurements, the OLED with **B2** showed deep blue emission with a high EQE_{max} of 18.3% at 1 cd m^{-2}, which fell to 12.6% at 100 cd m^{-2}. Compared to the PL spectrum there was a 5 nm redshift coupled with a minor broadening (FWHM = 37 nm) of the EL spectrum. The corresponding CIE coordinates are (0.13, 0.11), which
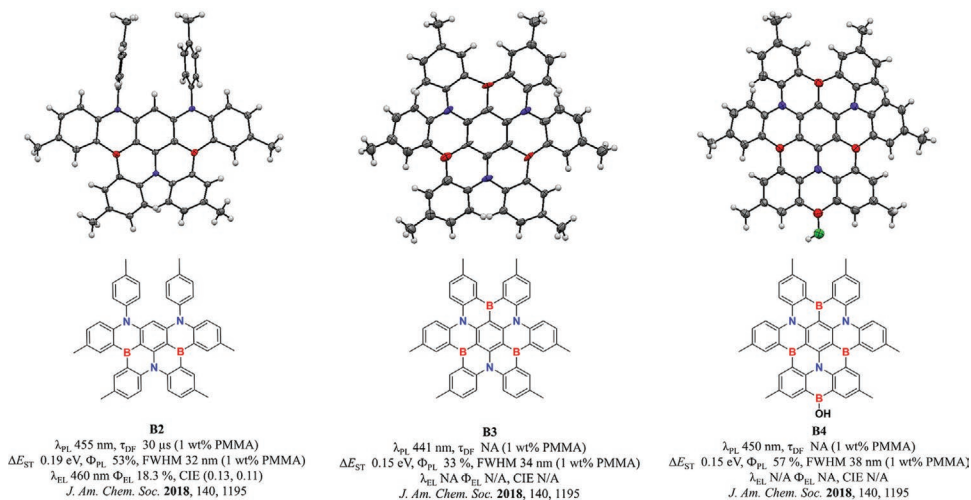

B2
λ_{PL} 455 nm, τ_{DF} 30 μs (1 wt% PMMA)
ΔE_{ST} 0.19 eV, Φ_{PL} 53%, FWHM 32 nm (1 wt% PMMA)
λ_{EL} 460 nm Φ_{EL} 18.3 %, CIE (0.13, 0.11)
J. Am. Chem. Soc. **2018**, 140, 1195

B3
λ_{PL} 441 nm, τ_{DF} NA (1 wt% PMMA)
ΔE_{ST} 0.15 eV, Φ_{PL} 33%, FWHM 34 nm (1 wt% PMMA)
λ_{EL} NA Φ_{EL} N/A, CIE N/A
J. Am. Chem. Soc. **2018**, 140, 1195

B4
λ_{PL} 450 nm, τ_{DF} NA (1 wt% PMMA)
ΔE_{ST} 0.15 eV, Φ_{PL} 57%, FWHM 38 nm (1 wt% PMMA)
λ_{EL} N/A Φ_{EL} NA, CIE N/A
J. Am. Chem. Soc. **2018**, 140, 1195

Figure 5. Chemical structures, crystal structures, photophysical properties, and device performances of **B2**, **B3**, and **B4**. Thermal ellipsoids are displayed in 50% probability. Adapted with permission.[29a] Copyright 2018, American Chemical Society.
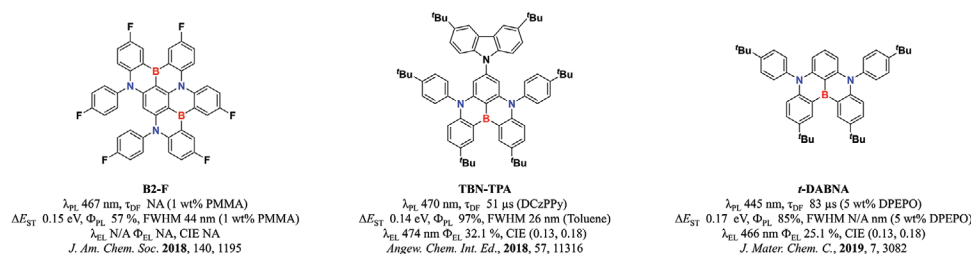
Figure 6. Chemical structures, photophysical properties, and device performances of **B2-F**, (Adapted with permission.[29a] Copyright 2018, American Chemical Society) **TBN-TPA** (Adapted with permission.[36] Copyright 2018, Wiley-VCH), and **t-DABNA** (Adapted with permission.[38] Copyright 2019, Royal Society of Chemistry).

are slightly redshifted compared to the CIE coordinates of (0.14, 0.08) in PMMA thin film. At 100 cd m^{-2}, the η_c and η_p were noted to be 11.5 cd A^{-1} and 7.1 lm W^{-1}. The color purity of the device is generally excellent, though the maximum luminance achieved was suboptimal at <1000 cd m^{-2}.

In 2018, Huang and co-workers[36] modified the structure of **DABNA-1** by incorporating a donor carbazole unit para to the boron acceptor (**TBN-TPA**; Figure 6) in order to improve the efficiency of the OLED. In their previous report, Hatakeyama et al. demonstrated how the multiresonant core of **DABNA-1** can be modified to improve its emission properties by functionalization with phenyl units and a diphenylamine moiety to generate **DABNA-2**. At the expense of color purity, they achieved a significant improvement in the PL and EL performance. The same structural design strategy is implemented by Huang and co-workers in their molecule (**TBN-TPA**) which is a derivative of **DABNA-1** but with *tert*-butyldiphenylamine units and containing a di-*tert*-butylcarbazole substituent para to the central boron atom. The target molecule was synthesized in three steps. The key reaction sequence, insertion of boron and cyclization, was done in one step. The presence of the electron-donating di-*tert*-butylcarbazole activates the arene substrate to electrophilic borylation. Even with the presence of this activating group, the overall yield of this reaction remains low at 26%. Even though **TBN-TPA** is a derivative of **DABNA-1**, its absorption spectrum exhibited distinguished bands at 451, 389, and 306 nm, which indicate the involvement of the di-*tert*-butylcarbazole in these bands. This lowest-energy transition corresponds to the absorption band at 451 nm in toluene, which is closer to that observed for the **DABNA-1** core (λ_{abs} = 437 nm) for which the HOMO and LUMO orbitals are localized on the DABNA core.[27a] The PL spectrum of **TBN-TPA**[36] in toluene is redshifted by 20 nm from that of **DABNA-1**,[29b] with a slightly broader emission profile with FWHM of 26 nm. The ΔE_{ST}, determined from the onset of the fluorescence and phosphorescence spectra in toluene, is 0.14 eV. The high oscillator strength combined with the small ΔE_{ST} translated into almost unity (Φ_{PL} = 97%) Φ_{PL} in toluene solution. Both the prompt and delayed lifetimes of **TBN-TPA** (τ_F = 6.01 ns, τ_D = 51.02 µs doped in 2,6-bis[3-(9*H*-carbazol-9-yl)phenyl]pyridine) (2,6-DCzPPy) are shorter than those of **DABNA-1** (τ_F = 8.8 ns, τ_D = 93.7 µs in mCBP film).[27a]

The EL spectrum of **TBN-TPA** remained narrow (FWHM = 27 nm) and showed a 4 nm redshift from its PL spectrum in toluene. However, the color purity is adversely affected, and in a similar manner to that observed for the OLED with **DABNA-2**, with CIE coordinates of (0.13, 0.19), which implicates a

change in the CIE$_y$ coordinate of 0.09. Employing a very different device architecture than that of the OLEDs fabricated in the **DABNA** series, the devices with **TBN-TPA** in the device configuration ITO/MoO$_3$ (2.5 nm)/(di-[4-(*N*,*N*-ditolyl-amino)-phenyl]cyclohexane (TAPC), 30 nm)/2,6-DCzppy: 4 wt% **TBN-TPA** (10 nm)/1,3,5-tri(*m*-pyrid-3-yl-phenyl)benzene (TmPyPB), 30 nm)/LiF(1 nm)/Al (100 nm) showed impressive performance: maximum luminescence was marked at 16 593 cd m^{-2} and the EQE$_{max}$ = 32.1%, albeit at low luminance. Strikingly, the EQE remained high at 13.9% even at its peak luminance of 16 593 cd m^{-2}. The maximum CE and PE for this device were 40.2 cd A^{-1} and 30.0 lm W^{-1}, respectively. At a practical brightness of 100 cd m^{-2}, the device based on **TBN-TPA** presented impressive efficiency values of EQE, CE, and PE of 27.4%, 34.4 cd A^{-1} and 23.5 lm W^{-1}, respectively, while device metrics with the parent compound (**DABNA-1**) were poor (EQE >10%),[27a] though a different device stack was used. In addition, **TBN-TPA** was employed as host for a phosphorescent yellow OLED having a device configuration ITO (50 nm)/HATCN (5 nm)/TAPC(30 nm)/**TBN-TPA**: 16 wt% Ir(tfmphqz)$_2$(tpip)[37] (10 nm)/TmPyPB (30 nm)/LiF (1 nm)/Al (100 nm). The improved carrier injection and film-forming ability of this compound is underlined by the impressive performance of the fabricated device, which showed a lower turn-on voltage (3.2 V), higher luminance (30 339 cd m^{-2}) and EQE$_{max}$ (22.2%), and with a very small efficiency roll-off compared to the device with 2,6-DCzppy as the host.[37] The Maximum CE and PE was measured to be 79.1 cd A^{-1} and 67.1 lm W^{-1}.

Later, Lee and co-workers have introduced **t-DABNA**, a modified version of **DABNA-1** with *tert*-butyl groups located para to the nitrogen atoms.[38] Following Hatakeyama's reported synthesis, **t-DABNA** was synthesized in two steps and in similar yields to that of the original report.[27a] The authors aimed at reducing the severe efficiency role off experienced by DABNA-type molecules, and especially **DABNA-1**, in devices. The introduction of the *tert*-butyl groups was expected to reduce intermolecular interactions in the emissive layer, thereby reducing the aggregation-caused quenching that is frequently observed in thin films of these materials at more elevated doping concentrations. The **t-DABNA** exhibited similar photophysical properties to the parent **DABNA-1**, but showing an expected modest redshift of 5 nm in the emission maximum. The ΔE_{ST} is slightly smaller for **t-DABNA** (0.17 eV) compared to that of **DABNA-1** (0.19 eV).[27a,38] Initial devices were fabricated with emitter doped in DPEPO as the host. At 5 wt% emitter concentration, the OLEDs with **t-DABNA** and **DABNA-1** exhibited

**ADVANCED
SCIENCE NEWS**
www.advancedsciencenews.com

**ADVANCED
FUNCTIONAL
MATERIALS**
www.afm-journal.de

EQE_{max} of 25.1% and 18.7%, respectively. The improved performance of *t*-DABNA was ascribed by the authors to its higher Φ_{PL} and reduced intermolecular interactions, which is underlined by the independence of Φ_{PL} on doping concentration. However, the two devices both suffered from serious efficiency roll-off and the device stability was poor, which were associated to the long-delayed fluorescence lifetimes of the emitters (τ_d = 83.3 μs in 5 wt% DPEPO). Appreciating the potential of MR-TADF emitters in OLEDs, the authors circumvented this issue by introducing DMAC-DPS as a TADF assistant dopant that can upconvert the triplet excitons and transfer energy to the emitter through Förster energy transfer and either **DABNA-1** or *t*-DABNA (Figure 6) as the emitter. DMAC-DPS is a well-known efficient blue TADF compound[39] possessing a short τ_d (5.6 μs), high triplet energy (2.91 eV), a fast rISC rate (2.53×10^5 s^{-1}) and was chosen as the assistant dopant as its absorption spectrum overlapped with the PL spectrum of the MR-TADF compounds, providing a route for efficient energy transfer. The authors named their energy transfer mechanism TATADF (TADF-assisted TADF). The solution-processed device stack was ITO/poly(3,4-ethylene dioxythiophene):poly(styrenesulfonate) (PEDOT:PSS, 60 nm)/ TAPC, 20 nm)/mCP, 10 nm/emitting layer (25 nm)/TSPO1, 5 nm/TPBi, 20 nm/LiF, 1.5 nm/Al, 200 nm. The emitting layer structures of the *t*-DABNA and **DABNA-1** devices consisted of DPEPO:*t*-DABNA and DPEPO:**DABNA-1** (25 nm, 1, 3, 5, or 10 wt%) and those of the TATADF devices were DPEPO:DMAC-DPS:*t*-DABNA and DPEPO:DMAC-DPS:**DABNA-1** (25 nm, 30 wt%, 1 wt%). The devices contained 30 wt% assistant dopant and 1 wt% emitter employed OLEDs exhibited performances showing EQE_{max} of 31.4% and 23.5% at 1 cd m^{-2} employing, respectively *t*-DABNA and **DABNA-1**. Even at a luminance of 1000 cd m^{-2} the device EQE remained high at 19.8% and 15.6%, respectively, using *t*-DABNA and **DABNA-1**. On the other hand, DPEPO: *t*-DABNA/**DABNA-1** based devices exhibited EQE_{max} values of 25.1% and 18.7%. The improved device efficiency was associated with the reduced concentration of long-lived triplet excitons in the MR-TADF emitter, which was demonstrated by studying the time-resolved PL decay analysis of films with and without the assistant dopant. The films without assistant dopant exhibited a long τ_d while the one with assistant dopant possessed a comparatively short τ_d coupled with a decrease in delayed fluorescence intensity associated with the energy transfer. The higher efficiency from *t*-DABNA based TATADF devices is in part due to its more horizontal orientation (horizontal dipole orientation ratio = 0.79) in the emissive layer. However, the transient PL analysis suggests that even with the high concentration of DMAC-DPS the long-lived delayed component of the emission decay remains. A comparison of the device lifetimes at 100 cd m^{-2} was made using *t*-DABNA with and without assistant TADF dopant. Even though the TATADF device presented a tenfold increase in lifetime over the other device, the lifetime was only just over 30 h (LT$_{50}$). According to the authors, the device lifetime can be further improved by selecting a more stable host and assistant dopant.

In an endeavor to achieve stable device using an emitter based on the DABNA core, the same group introduced another strategy wherein the DABNA core is employed as a fluorescent emitter in the OLED rather than utilizing them as TADF materials.[40] In order to mitigate against the long delayed lifetime of TADF emitters, which has been identified as deleterious for device stability, the authors designed an energy transfer scheme that permitted quenching of the triplet excitons generated upon electrical excitation by using an anthracene based fluorescent high band gap host α-AND (E_g = 3.15 eV, E_T = 1.73 eV).[40] The E_T of the host α-AND is lower than that of *t*-DABNA (E_g = 2.80 eV, E_T = 2.63 eV) and **DABNA-1** (E_g = 2.82 eV, E_T = 2.63 eV) and as a consequence triplets on the emitter are back energy transferred to the fluorescent host rather than undergoing rISC to the singlet excited state of the emitter. At a doping concentration of 3 wt% of emitter in the host, this energy transfer process dominates as indicated by a very weak emission from the host in the PL spectrum; no delayed emission was observed from the emitter. Devices were fabricated using 1–5% of emitter in the emissive layer in a Device configuration of (ITO, 50 nm)/*N,N,N′N′*-tetra[(1,1′-biphenyl)-4-yl]-(1,1′-biphenyl)-4,4′-diamine (BPBPA):HATCN(40 nm:30 wt%)/BPBPA (10 nm)/9,9-dimethyl-10-(9-phenyl-9H-carbazol-3-yl)-9,10-dihydroacridine (PCzAC) (10 nm)/α-ADN: (30 nm:3 wt% emitter)/2,8-bis(4,6-diphenyl-1,3,5-triazin-2-yl) dibenzo[b,d]furan (DBFTrz) (5 nm)/2-[4-(9,10-di-naphthalen-2-yl-anthracen-2-yl)-phenyl]-1-phenyl-1H-benzimidazole (ZADN) (20 nm)/LiF (1.5 nm)/Al (200 nm). A pyrene-based compound 4,4′-(pyrene-1,6-diylbis(phenylazanediyl))dibenzonitrile (PyCN) was used as a reference emitter in this case. Just like their previous report,[38] the *tert*-butyl-modified **DABNA-1**, *t*-DABNA (Figure 6) performed better in OLEDs compared to **DABNA-1**. Blue narrow-band emission with CIE$_y$ < 1 were achieved in the device stack. The corresponding EQE/CE at 1000 cd m^{-2} for devices based on **DABNA-1**, *t*-DABNA and PyCN were 4.9/3.4, 7.0/5.8, and 3.4/2.8, respectively. Device lifetime measurements at 200 cd m^{-2}, revealed LT$_{90}$ values of 608 h for the *t*-DABNA device whereas for the OLEDs with **DABNA-1** and PyCN lifetimes were significantly lower at 203 and 33 h respectively.

The same group continued to work on the device architecture to boost the EL performance of *t*-DABNA based devices. The authors introduced a phosphorescence-sensitized TADF (PSTADF) device to harvest triplet excitons without transferring energy into the triplet state of the MR-TADF emitter.[41] This type of energy transfer process has been previously used for other TADF emitters.[42] Unlike the previously discussed device,[40] dark triplets are converted into singlets here. It was noted that both efficiency and device lifetime were significantly improved compared to the previous devices with *t*-DABNA while simultaneously maintaining its deep blue emission. Devices were fabricated with TSPO1 host with 3% *t*-DABNA as emitter in the device configuration ITO, 50 nm/PEDOT:PSS, 60 nm/TAPC, 20 nm/ mCP, 10 nm/emitting layer, 25 nm/TSPO1, 5 nm/TPBi, 20 nm/ LiF, 1.5 nm/Al, 200 nm. The devices without inclusion of the phosphorescent sensitizer presented poor performance in terms of brightness (<500 cd m^{-2}) and efficiency roll off (EQE$_{100}$ = 4.5%). The authors investigated this energy transfer scheme with three different iridium-containing phosphorescent materials, *fac*-tris(3-(1-(2,6-diisopropylphenyl)-1H-imidazol-2-yl)-benzonitrile)iridium (CNImIr),[43] *fac*-tris(1-(2,6-diisopropylphenyl)-2-(4-fluorophenyl)-1H-imidazole)iridium (F-Ir)[43] and *fac*-tris(5-(tertbutyl)-1,3-diphenyl-2,3-dihydro-1H-imidazo[4,5-b]pyrazine)iridium (Ir(cb)$_3$).[44] The best sensitizer for *t*-DABNA was identified as Ir(cb)$_3$ from the favorable spectral overlap of sensitizer emission

v-DABNA
λ_{PL} 467 nm, τ_{DF} 4.1 μs (1 wt% in DOBNA-OAr)
ΔE_{ST} 0.017 eV, Φ_{PL} 90%, FWHM 18 nm (1 wt% in DOBNA-OAr)
λ_{EL} 469 nm Φ_{EL} 34.4 %, CIE (0.12, 0.11)
Nat. Photonics **2019**, 13, 678.

DOBNA-OAr
λ_{PL} 388 nm, τ_{DF} NA (Toluene)
ΔE_{ST} 0.017 eV, Φ_{PL} 65%, FWHM 34 nm (Toluene)
λ_{EL} NA Φ_{EL} NA, CIE NA
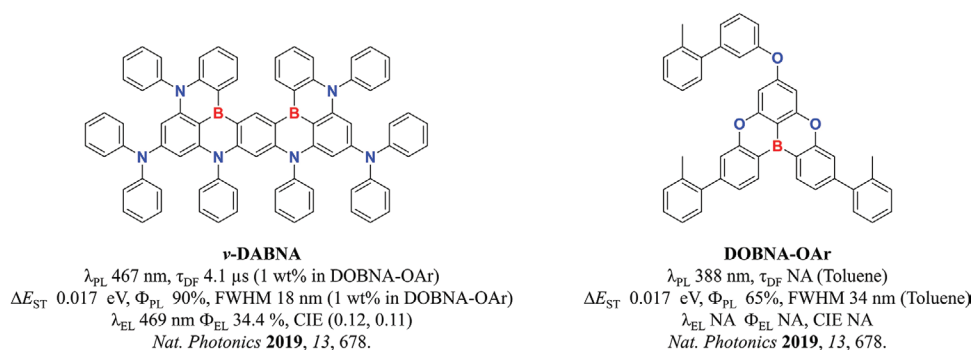*Nat. Photonics* **2019**, 13, 678.

Figure 7. Chemical structures, photophysical properties, and device performances of **v-DABNA** and **DOBNA-OAr**. Adapted with permission.[29b] Copyright 2019, Springer Nature.

and the absorption of **t-DABNA**. Complete energy transfer occurred in this case and only emission from **t-DABNA** was observed. This is also reflected in the fabricated device with an Ir(cb)$_3$ concentration of 30 wt% and **t-DABNA** doping at 0.5, 1, and 2 wt%. Pure blue emission with a CIE$_y$ of (<0.13) resulted from all the device in this series. Devices with other phosphorescent sensitizers exhibited mixed emission from the sensitizer and the MR-TADF emitter. The maximum luminescence noted for the best device (0.5 wt% **t-DABNA**) was 5019 cd m^{-2}. The EQE/CE/PE for devices with 0.5, 1, and 2 wt% emitter at 1000 cd m^{-2} were 19.4%/18.7 cd A^{-1}/9.7 lm W^{-1}, 18.4%/16.7 cd A^{-1}/8.5 lm W^{-1}, and 16.3%/14.5 cd A^{-1}/7.0 lm W^{-1}, respectively. For the lifetime studies, TSPO1 host was replaced with the more stable mCBP host, and the emitter doping concentration was set to 1 wt%. The EQE was slightly reduced to 14.2% at 1000 cd m^{-2}. The LT$_{50}$ was measured to be 293 h at 200 cd m^{-2}. The device stability was found to be significantly higher for the TATADF devices introduced in their earlier report,[40] which indicates further efforts are required to obtain both stable OLEDs at high efficiencies when employing MR-TADF emitters.

Expanding beyond triangulene structures is the recent report by Hatakeyama and co-workers of a pseudolinear MR-TADF compound, **v-DABNA** (Figure 7).[29b] Notably, the FWHM of **v-DABNA** is just only 14 nm in toluene, which is the narrowest of all the MR-TADF compounds reported so far. The extremely narrow emission band is attributed to the weak vibronic coupling to stretching modes in the S$_1$ excited state, so that the ground and excited states actually feature similar equilibrium geometries. The emission color of this compound is similar to those of the DABNA series of emitters previously reported by the same group. This molecule was synthesized in three steps in good yields in a similar manner to their previous report.[29a]

This report[29b] also introduces a new oxygen-bridged boron-centered high band gap host (**DOBNA-OAr**) for **v-DABNA**, which is itself based on the previously reported structure of **2a** (Figure 2). In dilute toluene solution, the emission maximum of the host is λ_{PL} = 388 nm (FWHM = 34) with an associated high Φ_{PL} of 65%. The absolute Φ_{PL} of a 1 wt% doped film of **v-DABNA** in **DOBNA-OAr** is 90%, which is higher than that of **v-DABNA** in dilute toluene solutions (74%). The ΔE_{ST} value of **v-DABNA** is miniscule at only 0.017 eV, which is the smallest among MR-TADF compounds reported to date. The calculated k_F, k_{IC}, k_{ISC}, and k_{RISC} from the transient decay spectra of **v-DABNA** in doped film are, respectively, 2.0 × 10^8, 2.2 × 10^7,

2.3 × 10^7, and 2.0 × 10^5 s^{-1}. Strikingly, there is an approximate 20- and 13-fold improvement in the k_{RISC} noted for **v-DABNA** versus **DABNA-1** and **DABNA-2**, respectively, which is the result of the significantly smaller ΔE_{ST} (0.017 eV). From an Arrhenius analysis[45] of k_{RISC} versus 1/T, the activation energy for RISC was estimated to be 0.07 eV, which is higher than the calculated ΔE_{ST} determined from the steady-state fluorescence and phosphorescence spectra, indicating a potential contribution of higher triplet energy levels (T_n) aiding the RISC process in **v-DABNA**.[25,46] It is noteworthy that this emitter presented a very short delayed lifetime (τ_F = 4.1 ns and τ_{TADF} = 4.1 μs).

The OLED with a device structure of ITO, 50 nm/NPD, 40 nm/TCTA, 15 nm/mCP, 15 nm/1 wt% **v-DABNA** in **DOBNA-OAr**, 20 nm/TSPO1, 30 nm/LiF, 1 nm/Al, 100 nm showed pure blue emission (λ_{EL} = 469 nm) with a record small FWHM of only 18 nm. The corresponding CIE coordinates are (0.12, 0.11). Strikingly, the device showed excellent efficiencies with an EQE$_{max}$ of 34.4% at a luminance of 15 cd m^{-2}. The efficiency roll-off was also much lower than those of most MR-TADF-based devices with EQEs of 32.8% and 26.0% at 100 and 1000 cd m^{-2}, respectively, corresponding to an efficiency drop of 1.6% and 8.6% at 100 and 1000 cd m^{-2}, respectively. The impressive performance of the OLED suggests that bimolecular quenching processes such as triplet-triplet and singlet–triplet annihilation are largely suppressed. Unfortunately, the emission intensity is drastically reduced after 31 h, but without spectral change, and thus efforts are still required to improve the device performance.

This blue emitter (**v-DABNA**) was utilized in a different way by Adachi and co-workers in an exciplex-forming OLED device through an exciton recycling strategy.[47] The role of **v-DABNA** in this case was to act as a fluorescent emitter for a TADF acceptor-based exciplex-forming host. The main focus of this report was to demonstrate the exciton recycling efficiency of their exciplex-forming host rather than utilizing the TADF property of **v-DABNA**. Even though the efficiency of doped devices (1 wt% **v-DABNA** in 49.5 wt% Tris-PcZ:49.5 wt% 3Cz-TRZ) was higher (EQE$_{max}$ = 19%) than that of nondoped devices, the overall device performance was inferior to that of the original **v-DABNA**-based device developed by Hatakeyama et al. This exciplex device also suffered from a significant emission redshift (CIE$_y$ = 0.36) and band-broadening (FWHM = 50 nm) compared to the pure blue emission based on the original **v-DABNA** device. The **v-DABNA** doped exciplex device lifetime was 300 h (LT$_{50}$) at a high luminescence of 1260 cd m^{-2}.

TCz-BN
λ_{PL} 477 nm, τ_{DF} N/A (Tol.)
ΔE_{ST} N/A, Φ_{PL} N/A, FWHM 22 nm (Tol.)
λ_{EL} 474 nm Φ_{EL} 18.9%, CIE (0.13, 0.20)
Angew. Chem. Int. Ed., **2019**, 18, 16912

2F-BN
λ_{PL} 502 nm, τ_{DF} 25.9 μs (6 wt% mCPBC film)
ΔE_{ST} 0.16 eV (tol.), Φ_{PL} 89% FWHM 32 nm (6 wt% mCPBC film)
λ_{EL} 501 nm Φ_{EL} 22.0%, CIE (0.16, 0.60)
Angew. Chem. Int. Ed., **2019**, 18, 16912

3F-BN
λ_{PL} 503 nm, τ_{DF} 16.7 μs (6 wt% mCPBC film)
ΔE_{ST} 0.08 eV (tol.), Φ_{PL} 83% FWHM 33 nm (6 wt% mCPBC film)
λ_{EL} 499 nm Φ_{EL} 22.7%, CIE (0.20, 0.58)
Angew. Chem. Int. Ed., **2019**, 18, 16912

4F-BN
λ_{PL} 501 nm, τ_{DF} 19.0 μs (6 wt% mCPBC film)
ΔE_{ST} 0.11 eV (tol.), Φ_{PL} 91% FWHM 31 nm (6 wt% mCPBC film)
λ_{EL} 493 nm Φ_{EL} 20.9%, CIE (0.12, 0.48)
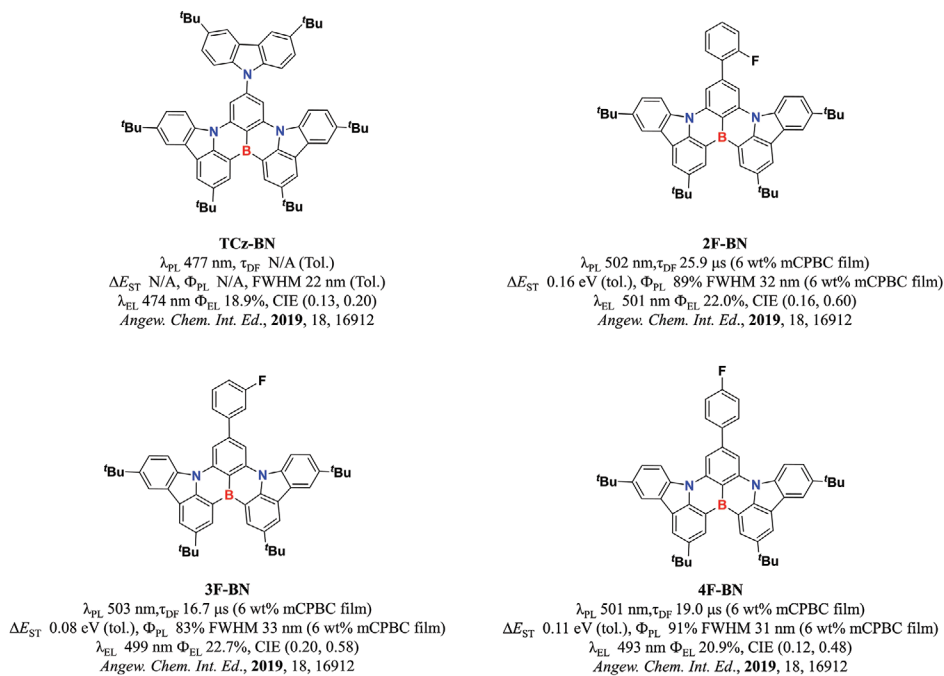*Angew. Chem. Int. Ed.*, **2019**, 18, 16912

Figure 8. Chemical structures, photophysical properties, and device performances of **TCz-BN**, **2F-BN**, **3F-BN**, and **4F-BN**. Adapted with permission.[48] Copyright 2019, Wiley-VCH.

A new series of B,N-doped nanographenes with a more extended π-conjugation than exists in **DABNA** series was recently reported by Duan and co-workers[48] The design includes the replacement of diphenyl amine units in **DABNA-1** with *tert*-butyl carbazole (**Figure 8** and the incorporation of isomeric fluorobenzene electron-withdrawing units. **2F-BN**, **3F-BN**, and **4F-BN**[27a] were synthesized following previous reports.[27a] Introduction of the fluorobenzene groups induces a charge transfer character to the HOMO-LUMO transition. Owing to the rigid structural framework, the reported emitters showed small FWHM's (22–25 nm) and high Φ_{PL}'s (90–99%) in dilute toluene solution. These three compounds show green emissions (501–503 nm) with Φ_{PL}'s ranging from 83 to 91% in 6 wt% films in 9-(3-(9H-carbazol-9-yl) phenyl)-9H-3,9'-bicarbazole (mCPBC). The ΔE_{ST} and τ_d values are 0.16, 0.08, and 0.11 eV and 25.9, 16.7, and 19.0 μs, respectively. The delayed lifetimes are shorter than that of **TCz-BN**.[27a] As expected from their PL spectra, all three compounds exhibited green emission in the thin film. Devices were fabricated with the configuration ITO/HAT-CN,10 nm/N,N'-di(1-naphthyl)-N,N'-diphenyl-(1,1'-biphenyl)-4,4'-diamine (NPB), 30 nm/BCzPh, 10 nm/EML, 20 nm/9Cz46Pm, 10 nm/DPPyA:Liq (1:1), 30 nm/LiF, 0.5 nm/Al, 150 nm. A mixed host system (mCPCB: 35 wt% 2,3,4,5,6-pentakis-(3,6-di-*tert*-butyl-9H-carbazol-9-yl) benzonitrile (5TCzBN)) was used for their device. The optimized concentration of the emitter in the device was 9 wt% for **2F-BN** and 6 wt% for both **3F-BN** and **4F-BN**. The λ_{EL} exhibited are 501 nm (FWHM = 40 nm), 499 nm (39 nm), and 493 nm (32 nm), respectively for **2F-BN**, **3F-BN**, and **4F-BN**. The OLED with **2F-BN** presented an impressive CIE$_y$ coordinate of 0.60, which is a real advance toward achieving green for MR-TADF compounds.[17] The

emitters also exhibited good device performances, with EQE$_{max}$ (PE$_{max}$) values of 22.0 (69.8 lm W^{-1}), 22.7 (72.3 lm W^{-1}) and 20.9% (51.3 lm W^{-1}) for **2F-BN**, **3F-BN**, and **4F-BN**, respectively. Due to their fused planar structure, the devices fabricated with these new emitters also exhibited excimer emission. The OLEDs using each of these three emitters showed small efficiency roll-off. The EQE$_{1000}$ are 15.0%, 21.1%, and 16.4% for **2F-BN**, **3FBN**, and **4F-BN**, respectively. The OLEDs showed lifetimes (LT$_{90}$) of 45.76, 15.53, and 10.35 h for **2F-BN**, **3F-BN**, and **4F-BN**, respectively, at a high initial luminescence of 2000 cd m^{-2}.

Inspired from the results of our computational studies (vide infra) on linear MR-TADF compounds,[49] we designed and synthesized a deep blue-emitting, linear, ladder type B,N doped heptacene (**α-3BNOH**) and investigated its photophysical properties (**Figure 9**).[50] B,N-doped ladder-type acenes had been previously identified as highly fluorescent materials by Agou et al.[51] However, the previous report did not recognize that these compounds fall within the family of MR-TADF emitters. **α-3BNOH** was obtained from a one pot triple electrophilic borylation at high temperature using a similar protocol to the one developed by Hatakeyama and co-workers[29a] High thermal stability was observed for **α-3BNOH** (T_d = 554 °C). The λ_{PL} is 390 nm with a narrow FWHM of 31 nm in THF solutions, Φ_{PL} under N$_2$ is 50%. Unlike **ν-DABNA** or other MR-TADF emitters, ΔE_{ST} for this emitter was found to be on the higher side (0.31 eV) in solution. Temperature-dependent PL decay measurements indicated that aggregates are formed at low temperature in THF glass, which facilitates delayed emission from a TTA process. This is surprising considering that the emission measurements were done at very high dilution. The TADF component becomes dominant at 300 K. Direct determination of the
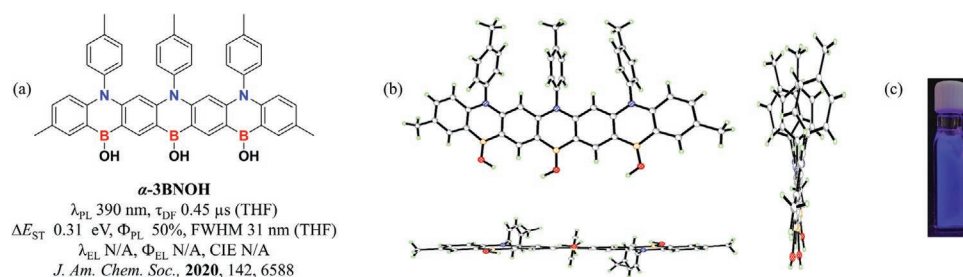
Figure 9. a) Chemical structure and photophysical properties of *α*-3BNOH. b) Crystal structure. Thermal ellipsoids are displayed in 50% probability. c) Emission of *α*-3BNOH in dilute THF under UV at 300 K. Adapted with permission.[50] Copyright 2020, American Chemical Society.

activation energy for the delayed emission is only 70 meV while the ΔE_{ST} was calculated to be 310 meV. Similar behavior was observed in other TADF reports[52] including for *ν*-DABNA.[29b] This dichotomy can be explained by invoking contributions from higher-lying triplet states to the RISC process, which is supported by our computations. The delayed lifetime in solution was found to be the shortest (0.45 µs) of all the MR-TADF emitters reported to date. In 1 wt% PMMA film of *α*-3BNOH, emission is slightly redshifted to 395 nm (FWHM = 32 nm) from the solution state, and ΔE_{ST} becomes smaller at 0.22 eV. It is noteworthy that this emitter presented an impressive CIE_y coordinate of 0.01 in 1 wt% doped state in PMMA. In thin film, the activation energy matches with the calculated singlet–triplet energy gap. The delayed lifetime in the PMMA film is much longer at 260 µs. No devices were fabricated in this report with this emitter. To date, the family of MR-TADF compounds have all contained boron as the electron-poor atom, which, in the triangulene family of compounds, is always centrally located.[53]

Moving from acceptor-centered multiresonant emitters, Hatakeyama and co-workers reported donor-centered azadiboranaphthoanthracene derivatives (**ADBNA-Me Mes** and **ADBNA-Me-Tip**; **Figure 10**).[54] The core structure consist of two acceptor boron atoms each positioned *para* to a centrally located donor nitrogen atom. The synthesis of these two emitters is shown in **Scheme 3**. The intermediate tribromotriarylamine, which was obtained by electrophilic aromatic bromination of tri-4-tolylamine, was subjected to lithiation and boron insertion. Finally, the boranes were arylated using Grignard reagents. The overall yield was reported to be 27% and 14%, respectively for **ADBNA-Me-Mes** and **ADBNA-Me-Tip**. The photophysical properties of 1 wt% films of the two ABDNA derivatives were investigated using **DOBNA-OAr** as the host.[29b] Compare to **DABNA-1** (λ_{PL} = 460 nm, 1 wt% in mCBP),[27a] these compounds showed redshifted emission of 482 and 479 nm, respectively,

for **ADBNA-Me-Mes** and **ADBNA-Me-Tip**. Notably, the FWHM remained narrow (33 and 34, respectively for **ADBNA-Me-Mes** and **ADBNA-Me-Tip**). Their inclusion as multiresonant TADF compounds is evidenced by their small measured ΔE_{ST} (0.18 eV). The delayed lifetimes, τ_d, are 165 and 147 µs for **ADBNA-Me-Mes** and **ADBNA-Me-Tip**, respectively. The k_{RISC} values for **ADBNA-Me-Mes** (7.6×10^3 s^{-1}) and **ADBNA-Me-Tip** (9.0×10^3 s^{-1}) were noted to be similar to that of **DABNA-1** (11.1×10^3 s^{-1}). Compared to the pseudolinear diboron MR-TADF emitter *ν*-DABNA, the triangulene-based diboron emitters exhibited very long delayed fluorescence lifetimes in the same host with a similar Φ_{PL} values.[29b]

Devices were fabricated using the same host as for *ν*-DABNA, in the following architecture: ITO 50 nm/HAT-CN, 5 nm/NPB, 35 nm/TCTA, 15 nm/mCP, 15 nm/1 wt% ADBNA emitter and 99 wt% **DOBNA-OAr**, 20 nm/TSPO1, 40 nm/LiF, 1 nm/and Al, 100 nm. The OLEDs showed narrow-band sky-blue emission of 481 nm (FWHM = 32 nm) and 480 nm (FWHM = 33 nm), respectively for **ADBNA-Me-Mes** and **ADBNA-Me-Tip**. The corresponding CIE values are (0.10 0.27) and (0.11, 0.29) for **ADBNA-Me-Mes** and **ADBNA-Me-Tip**, respectively. Notably the device with **ADBNA-Me-Tip** showed an EQE_{max} of 21.4%, while with **ADBNA-Me-Mes** showed a slightly lower value of 16.2%. The improved efficiency of the device with **ADBNA-Me-Tip** was rationalized from its higher orientation parameter (S) of −0.40 versus −0.11 of **ADBNA-Me-Mes** based on angle-dependence PL measurements. However, the maximum brightness achieved with these devices are low, less than 1000 cd m^{-2}. Here too, large efficiency roll-offs were observed.

Recently, Wang and co-workers[55] reported a series of emitters based on an inverted **DABNA** design where the nitrogen donor is positioned centrally in the triangulene structure (**Figure 11**), structures that are similar to the ADBNA series[54] reported by Hatakeyama and co-workers. Synthesis was not as straightforward as previously reported MR-TADF emitters, with
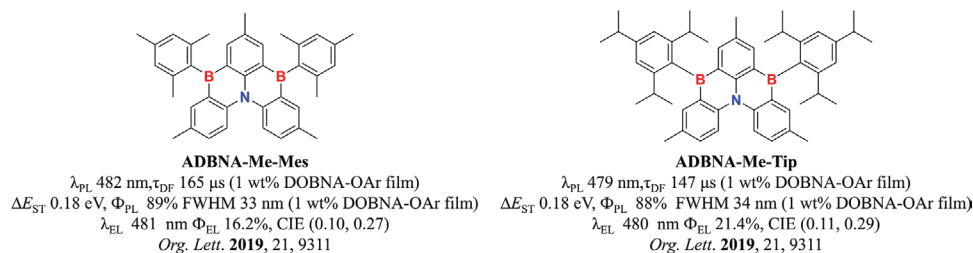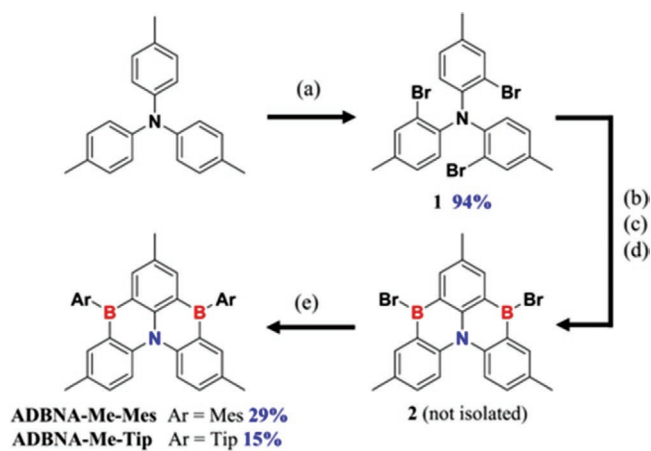

ADBNA-Me-Mes
λ_{PL} 482 nm, τ_{DF} 165 µs (1 wt% DOBNA-OAr film)
ΔE_{ST} 0.18 eV, Φ_{PL} 89% FWHM 33 nm (1 wt% DOBNA-OAr film)
λ_{EL} 481 nm Φ_{EL} 16.2%, CIE (0.10, 0.27)
Org. Lett. **2019**, 21, 9311

ADBNA-Me-Tip
λ_{PL} 479 nm, τ_{DF} 147 µs (1 wt% DOBNA-OAr film)
ΔE_{ST} 0.18 eV, Φ_{PL} 88% FWHM 34 nm (1 wt% DOBNA-OAr film)
λ_{EL} 480 nm Φ_{EL} 21.4%, CIE (0.11, 0.29)
Org. Lett. **2019**, 21, 9311

Figure 10. Chemical structures, photophysical properties, and device performances of **ADBNA-Me-Mes** and **ADBNA-Me-Tip**. Adapted with permission.[54] Copyright 2019, American Chemical Society.

**ADVANCED
SCIENCE NEWS**

www.advancedsciencenews.com

**ADVANCED
FUNCTIONAL
MATERIALS**

www.afm-journal.de

Scheme 3. Synthesis of inverted ADBNA derivatives: a) NBS (3.1 equiv.) CH$_3$CN, rt, 20 h, b) t-BuLi (6.1 equiv.) ^{t}Bu-benzene, −40 °C to rt, rt 1 h, c) BBr$_3$ (2.0 equiv.), 0 °C to rt, rt 1 h, d) 1,2,2,6,6-pentamethylpiperidine (2.0 equiv.), rt to 160 °C, 160 °C 15 h, and e) ArMgBr (3.0 equiv.), rt. Adapted with permission.[54] Copyright 2019, American Chemical Society.

direct conversion of N(B-tolyl)$_3$ to the target not possible with simple *trans*-metallation and insertion. Instead intermediate **1** (**Scheme 4**) was isolated and was subjected to borylation with BBr$_3$ to afford asymmetric intermediate **2a** and symmetric analog **2b**, the product ratio of which could be controlled by the stoichiometry of BBr$_3$ and the reaction times (Scheme 5). Using this protocol, a number of derivatives were synthesized (Figure 11). Previous attempts to make inverted DABNA-type structures are limited to symmetrical structures while the synthetic route developed in this report successfully generates unsymmetrical inverted DABNA derivatives. Compounds **3–5b** displayed PL features reminiscent of MR-TADF, showing narrow FWHM, and only a small degree of positive solvatochromism. Emission maxima ranged from 482 to 487 nm, and Φ_{PL} ranged from 71% to 88%. The family of emitters showed ΔE_{ST} of between 0.17 and 0.19 eV. A different story exists for **6a** and **6b**. Here, in DCM, two emission peaks were observed, one located at 477/481 and 609/601 nm, respectively. The bluer emission band is much more MR-TADF in nature, with narrow emission and moderate solvatochromism, whereas the low
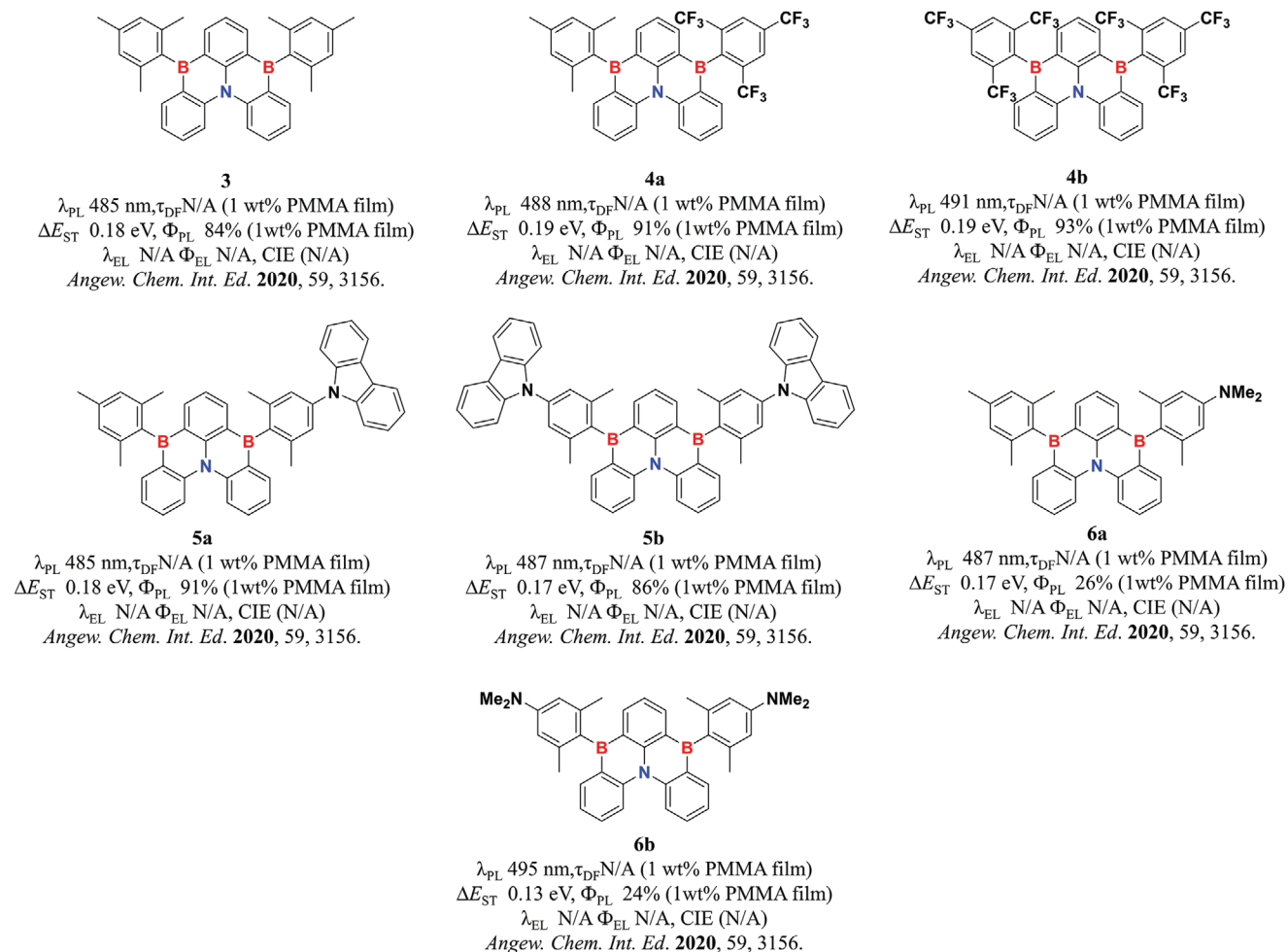

3
λ_{PL} 485 nm, τ_{DF} N/A (1 wt% PMMA film)
ΔE_{ST} 0.18 eV, Φ_{PL} 84% (1wt% PMMA film)
λ_{EL} N/A Φ_{EL} N/A, CIE (N/A)
Angew. Chem. Int. Ed. **2020**, 59, 3156.

4a
λ_{PL} 488 nm, τ_{DF} N/A (1 wt% PMMA film)
ΔE_{ST} 0.19 eV, Φ_{PL} 91% (1wt% PMMA film)
λ_{EL} N/A Φ_{EL} N/A, CIE (N/A)
Angew. Chem. Int. Ed. **2020**, 59, 3156.

4b
λ_{PL} 491 nm, τ_{DF} N/A (1 wt% PMMA film)
ΔE_{ST} 0.19 eV, Φ_{PL} 93% (1wt% PMMA film)
λ_{EL} N/A Φ_{EL} N/A, CIE (N/A)
Angew. Chem. Int. Ed. **2020**, 59, 3156.

5a
λ_{PL} 485 nm, τ_{DF} N/A (1 wt% PMMA film)
ΔE_{ST} 0.18 eV, Φ_{PL} 91% (1wt% PMMA film)
λ_{EL} N/A Φ_{EL} N/A, CIE (N/A)
Angew. Chem. Int. Ed. **2020**, 59, 3156.

5b
λ_{PL} 487 nm, τ_{DF} N/A (1 wt% PMMA film)
ΔE_{ST} 0.17 eV, Φ_{PL} 86% (1wt% PMMA film)
λ_{EL} N/A Φ_{EL} N/A, CIE (N/A)
Angew. Chem. Int. Ed. **2020**, 59, 3156.

6a
λ_{PL} 487 nm, τ_{DF} N/A (1 wt% PMMA film)
ΔE_{ST} 0.17 eV, Φ_{PL} 26% (1wt% PMMA film)
λ_{EL} N/A Φ_{EL} N/A, CIE (N/A)
Angew. Chem. Int. Ed. **2020**, 59, 3156.

6b
λ_{PL} 495 nm, τ_{DF} N/A (1 wt% PMMA film)
ΔE_{ST} 0.13 eV, Φ_{PL} 24% (1wt% PMMA film)
λ_{EL} N/A Φ_{EL} N/A, CIE (N/A)
Angew. Chem. Int. Ed. **2020**, 59, 3156.

Figure 11. Chemical structures and photophysical properties of **3**, **4a**, **4b**, **5a**, **5b**, **6a**, and **6b**. Adapted with permission.[55] Copyright 2020, Wiley-VCH.
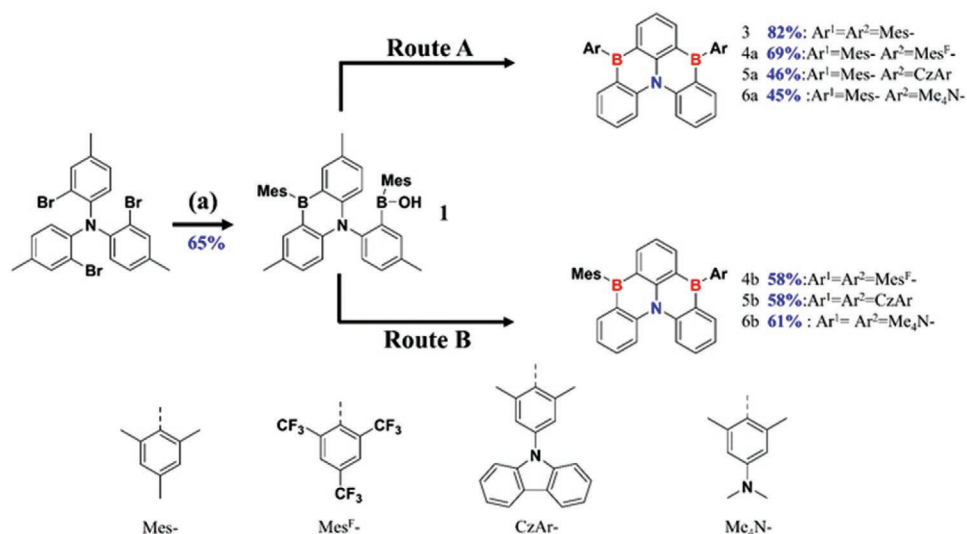
Scheme 4. Synthesis of inverted DABNA derivatives: a) t-BuLi, MesB(OMe)$_2$, THF, −78 °C, Route A: a) BBr$_3$ (1 equiv.), toluene, 110 °C, 1 h, b) Li–Ar (1.2 equiv.), THF/Et$_2$O, −78 °C → RT, 12 h. Route B: a) BBr$_3$ (5 equiv.), toluene, 110 °C, 24 h, b) Li–Ar (2.4 equiv.), THF/Et$_2$O, −78 °C → RT, 12 h. Adapted with permission.[55] Copyright 2020, Wiley-VCH.

energy emission band is more characteristic of that observed for CT type D–A materials. It is unclear at present why dual emission was observed only in these two compounds and not the others in the family. No devices were fabricated in this report to identify the EL performances of these new emitters.

The impact of the initial reports of MR-TADF compounds has spurred increased research efforts to design new MR-TADF emitters and donor–acceptor derivatives that rely on MR-TADF motifs which act as acceptor groups. One of such recent report by Meng et al.[56] employs **2a**[28] (Figure 2), previously reported by Hatakeyama and co-workers, as acceptor for donor–acceptor TADF emitters, in a similar design paradigm to that of **2e** (Figure 2), which used a phenoxazine donor.[28] The authors synthesized three regioisomers (**Figure 12**) having the same acceptor core (**2a**; Figure 2) and containing two electron donor units (dimethylacridine, DMAc). The impact of the position of donor substitution on the TADF properties were investigated: **m-AC-DBNA** (*meta* to boron and *para* to oxygen), **p-AC-DBNA** (*para* to boron and *meta* to oxygen) and **m′-AC-DBNA** (*meta* to boron and *ortho* to oxygen). **p-AC-DBNA** showed the highest temperature stability (T_d = 445 °C) and melting point (T_m = 436 °C) along with the highest Φ_{PL} (96%) and shortest τ_d (1.17 μs) in CH$_2$Cl$_2$ among the family of isomeric emitters; this isomer also showed the fastest k_{RISC} rate (1.2 × 10^5 s^{-1}) in 5 wt% doped BCPO films. Surprisingly, the emission maxima remain similar (λ_{PL} = 496 nm) compared to **m-AC-DBNA** (λ_{PL} = 492 nm) and **m′-AC-DBNA** (λ_{PL} = 498 nm) in doped film. As expected from their PL measurements, the OLED with
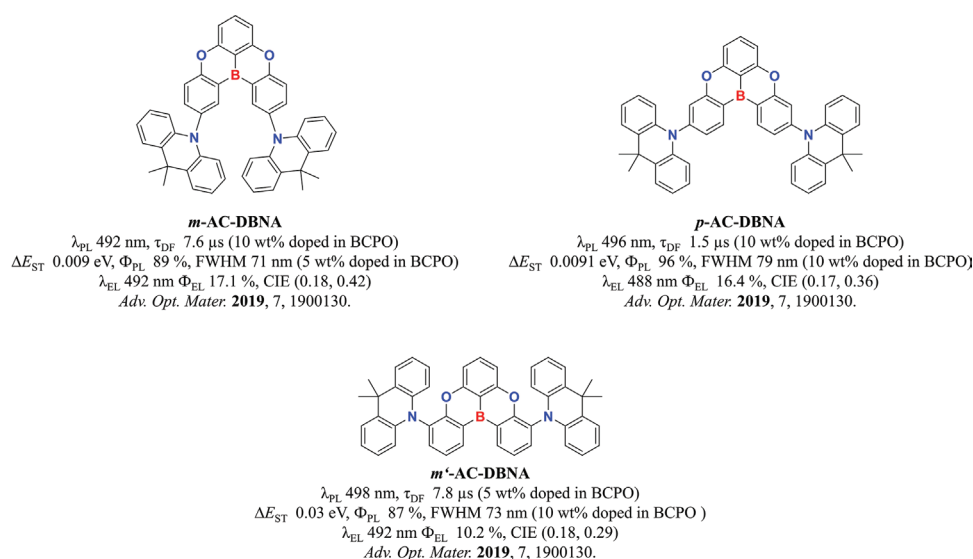

m-AC-DBNA
λ_{PL} 492 nm, τ_{DF} 7.6 μs (10 wt% doped in BCPO)
ΔE_{ST} 0.009 eV, Φ_{PL} 89 %, FWHM 71 nm (5 wt% doped in BCPO)
λ_{EL} 492 nm Φ_{EL} 17.1 %, CIE (0.18, 0.42)
Adv. Opt. Mater. **2019**, 7, 1900130.

p-AC-DBNA
λ_{PL} 496 nm, τ_{DF} 1.5 μs (10 wt% doped in BCPO)
ΔE_{ST} 0.0091 eV, Φ_{PL} 96 %, FWHM 79 nm (10 wt% doped in BCPO)
λ_{EL} 488 nm Φ_{EL} 16.4 %, CIE (0.17, 0.36)
Adv. Opt. Mater. **2019**, 7, 1900130.

m′-AC-DBNA
λ_{PL} 498 nm, τ_{DF} 7.8 μs (5 wt% doped in BCPO)
ΔE_{ST} 0.03 eV, Φ_{PL} 87 %, FWHM 73 nm (10 wt% doped in BCPO)
λ_{EL} 492 nm Φ_{EL} 10.2 %, CIE (0.18, 0.29)
Adv. Opt. Mater. **2019**, 7, 1900130.

Figure 12. Chemical structures, photophysical properties, and device performances of **m-AC-DBNA, p-AC-DBNA**, and **m′-AC-DBNA**. Adapted with permission.[56] Copyright 2019, Wiley-VCH.
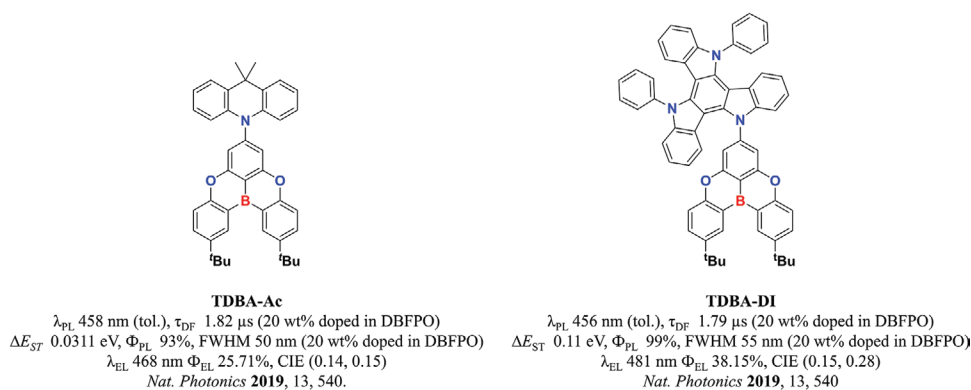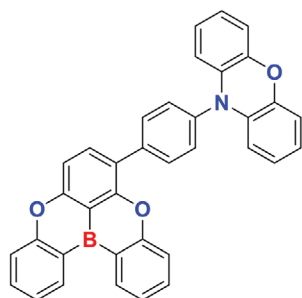
**ADVANCED
SCIENCE NEWS**

www.advancedsciencenews.com

**ADVANCED
FUNCTIONAL
MATERIALS**

www.afm-journal.de

TDBA-Ac
λ_{PL} 458 nm (tol.), τ_{DF} 1.82 μs (20 wt% doped in DBFPO)
ΔE_{ST} 0.0311 eV, Φ_{PL} 93%, FWHM 50 nm (20 wt% doped in DBFPO)
λ_{EL} 468 nm Φ_{EL} 25.71%, CIE (0.14, 0.15)
Nat. Photonics **2019**, 13, 540.

TDBA-DI
λ_{PL} 456 nm (tol.), τ_{DF} 1.79 μs (20 wt% doped in DBFPO)
ΔE_{ST} 0.11 eV, Φ_{PL} 99%, FWHM 55 nm (20 wt% doped in DBFPO)
λ_{EL} 481 nm Φ_{EL} 38.15%, CIE (0.15, 0.28)
Nat. Photonics **2019**, 13, 540.

Figure 13. Chemical structures, photophysical properties, and device performance of **TDBA-Ac** and **TDBA-DI**. Adapted with permission.[57] Copyright 2019, Springer Nature.

***p*-AC-DBNA** showed excellent EL performance in terms of turn-on voltage (3.3 V), maximum luminance (40 750 cd m^{-2}), and EQE$_{max}$ (20.5%). Devices were fabricated in the configuration, ITO/HATCN (4.2 nm)/TAPC (34 nm)/emission layer (23 nm)/TmPyPB (21 nm)/LiF (1 nm)/Al (100 nm). Even at higher luminescence of 1000 cdm^{-2}, devices based on ***p*-AC-DBNA** presented higher efficiency values (EQE = 16.4%). Due to the impressive device performance, the authors fabricated devices with different doping concentration (5–35 wt%) of emitters to identify the performance change. It was identified that 10 wt% emitter presented the best device performance in terms of efficiency. However, the maximum EQE was nearly insensitive to the doping concentration of the emitter. It is noted that at higher doping concentrations, efficiency roll off was significantly small (only 5% for 35% emitter vs 26% for 5% emitter) at the same time maximum brightness was dramatically increased (69 160 cd m^{-2} for 35% emitter vs 28 600 cd m^{-2} for 15% emitter). Impressed by the high performance of higher doping devices, this report also fabricated a nondoped device with the best emitter in this series, a low turn on voltage of 2.7 V was marked for this device with a red shift of emission. The expected efficiency boost was not observed for this device as evidenced by an EQE$_{max}$ of only 14.1 (efficiency roll off, 10%) with a maximum luminescence of 27 600 cd m^{-2}.

Kwon and co-workers[57] also explored the use of B,O-MR-TADF compounds as acceptors in D–A TADF emitters (**Figure 13**). Two emitters were designed in this report sharing the same boron-containing acceptor, a *tert*-butyl analog of **2a** (Figure 2), with two different donors: diindolocarbazole (**TDBA-DI**) and dimethylacridine (**TDBA-Ac**). TD-DFT calculations suggest that in these two emitters there is strong separation of the electron densities in the HOMO and LUMO thereby affording small calculated ΔE_{ST} of 0.006 and 0.073 eV for **TDBA-Ac** and **TDBA-DI**, respectively. As expected from the molecular design, both **TDBA-Ac** and **TDBA-DI** showed blue emission in dilute toluene with small ΔE_{ST} at 458 nm (0.06 eV) and 456 nm (0.11 eV), respectively, for **TDBA-Ac** and **TDBA-DI**. Associated with the small ΔE_{ST}, **TDBA-Ac** and **TDBA-DI**, respectively, possessed very short τ_d of 1.0 and 6.2 μs in toluene. They also showed that τ_d becomes shorter in more polar solvents, which is due to stabilization of the charge transfer band. Unlike MR-TADF emitters, these emitters do not sho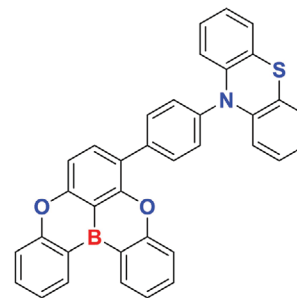w any concentration quenching when doped in films at high concentration (20 wt%). Similar values for k_{RISC} (9.9 × 10^5 and 1.1 × 10^6 s^{-1}) was inferred for **TDBA-Ac** and **TDBA-DI**, respectively. However, the nonradiative decay rate, k_{nr}, of **TDBA-Ac** (7.4 × 10^4 s^{-1}) was found to be higher than that of **TDBA-DI** (1.1 × 10^4 s^{-1}). Both the emitters were tested in an OLED device stack having a configuration of ITO/HATCN, 7 nm/TAPC, 50 nm/DCDPA, 10 nm/20% TADF emitter:host, 25 nm/dibenzo[b,d]furan-2,8-diylbis(diphenylphosphine oxide) (DBFPO), 10 nm/TPBi, 20 nm/LiF, 1.5 nm/Al, 100 nm. A high EQE$_{max}$ of 25.7% with a CIE of (0.14, 0.15) was observed for **TDBA-Ac** in the OLED using DBFPO as the host. When a less polar host such as 5-(5-(2,4,6-triisopropylphenyl)pyridin-2-yl)-5*H*-benzo[d]benzo[4,5]imidazo[1,2-a]imidazole (PPBI) was used in the device, the λ_{EL} (448 nm) blueshifted with the EL spectrum showing CIE of (0.15, 0.06) but the OLED showed a slightly lower EQE$_{max}$ of 21.5%. The difference in performance is more pronounced when the emitter is switched to **TDBA-DI**. The OLED showed EQE$_{max}$ of 32.2% and 38.2% with PPBI and DBFPO as hosts in the emissive layer, respectively. It is noteworthy that the DBFPO/**TDBA-DI** device exhibited a high luminance of 47 680 cd m^{-2} and also a very low efficiency roll-off to an EQE of 25.2% at 5000 cd m^{-2}. The authors demonstrated that the emitter orients horizontally in the thin film, and the improved light-outcoupling contributes to the outstanding EQEs of the OLED. The operational life (LT$_{50}$) of the same emitter/host system was short, less than 2 h at 500 cd m^{-2}, which was improved to 102.9 h by switching to a mixed host system of mCBP-CN:DDBFT; however, this was associated with a much lower EQE$_{max}$ of 22.3%.

Very recently, Song et al.[58] reported a series of D–π–A-type TADF emitters (**Figure 14**) having the same **2a** acceptor (Figure 2) core reported by Hatakeyama and co-workers[28] This family of emitters contains phenoxazine and phenothiazine donor units attached to the acceptor core through a phenyl linker. Unlike other D–A system using **2a** (Figure 2) as the acceptor, these molecules show different regiochemical substitution on the acceptor unit. Bromination of **2a** (Figure 2) occurs on the most electron-rich central ring. The brominated intermediate was then elaborated further via Suzuki–Miyaura coupling with boronic esters of donor units. Mono- and dibromination products of **2a** (Figure 2) were obtained using NBS as the bromination agent in 67% and 56% yields, respectively. The **OBO-O** and **OBO-S** emitters share the same acceptor and
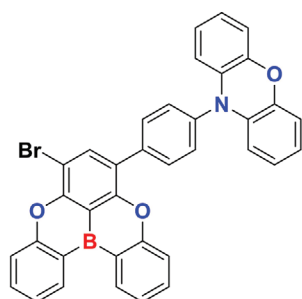
**ADVANCED
SCIENCE NEWS**
www.advancedsciencenews.com

**ADVANCED
FUNCTIONAL
MATERIALS**
www.afm-journal.de

OBA-O
λ_{PL} 450 nm, τ_{DF} 4.14 µs (10 wt% mCP film)
ΔE_{ST} 0.09 eV, Φ_{PL} 84% FWHM 80 nm (10wt% mCP film)
λ_{EL} 446 nm Φ_{EL} 17.8%, CIE (0.17, 0.17)
J. Mater. Chem. C **2019**, 7, 11953.

OBA-S
λ_{PL} 470 nm, τ_{DF} 4.8 (10 wt% mCP film)
ΔE_{ST} 0.09 eV, Φ_{PL} 75% FWHM 68 nm (10 wt% mCP film)
λ_{EL} 488 nm Φ_{EL} 4.4%, CIE (0.20, 0.31)
J. Mater. Chem. C **2019**, 7, 11953.

OBA-BrO
λ_{PL} 476 nm, τ_{DF} 3.74 µs (10 wt% mCP film)
ΔE_{ST} 0.04 eV, Φ_{PL} 92% FWHM 83 nm (10 wt% mCP film)
λ_{EL} 500 nm Φ_{EL} 22.5%, CIE (0.20, 0.38)
J. Mater. Chem. C **2019**, 7, 11953.
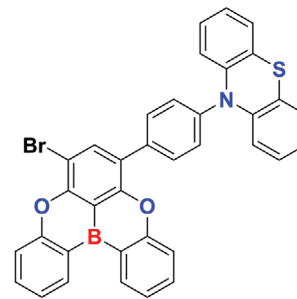
OBA-BrS
λ_{PL} 470 nm, τ_{DF} 0.81 µs (10 wt% mCP film)
ΔE_{ST} 0.07 eV, Φ_{PL} 55% FWHM 108 nm (10 wt% mCP film)
λ_{EL} 520 nm Φ_{EL} 9.2%, CIE (0.29, 0.46)
J. Mater. Chem. C **2019**, 7, 11953.

Figure 14. Chemical structures, photophysical properties, and device performances of **OBA-O**, **OBA-S**, **OBA-BrO**, and **OBA-BrS**. Adapted with permission.[58] Copyright 2019, Royal Society of Chemistry.

contain phenoxazine and phenothiazine donors, respectively. The **OBA-BrO** and **OBA-BrS** each contain an additional bromine substituent on the acceptor. In dilute toluene solutions, emission maxima ranged from 444 to 478 with Φ_{PL}'s of 53–84%. In line with previously reported D–A systems, the ΔE_{ST} values are very small, ranging from 0.04 to 0.09 eV in 10 wt% mCP films.

Devices were fabricated with the stack ITO/HATCN, 5 nm/ TAPC, 40 nm/3, 5, and 7 wt% emitter: mCP, 20 nm/TmPyPB, 40 nm/LiF, 1 nm/Al, 100 nm. The best OLED was obtained with **OBA-O** at 5 wt% emitter doping concentration, and this device was gratifyingly also the bluest (λ_{EL} = 446 nm, CIE = (0.17, 0.17)) of all the devices in this report. A low turn on voltage (2.7 V), high
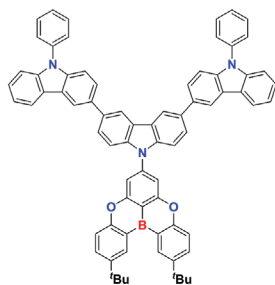
3CzTB
λ_{PL} 433 nm (tol), τ_{DF} 9.32 µs (20 wt% doped in DBFPO)
ΔE_{ST} 0.23 eV (tol), Φ_{PL} 88%, FWHM 49 nm (20 wt% doped in DBFPO)
λ_{EL} 470 nm Φ_{EL} 29.1%, CIE (0.14, 0.19)
J. Mater. Chem. C **2020**, 8, 2272.
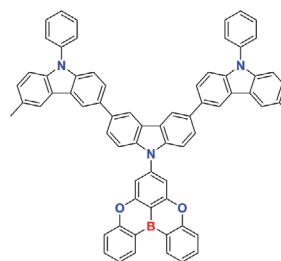
M3CzB
λ_{PL} 445 nm (tol), τ_{DF} 7.84 µs (20 wt% doped in DBFPO)
ΔE_{ST} 0.14 eV (tol), Φ_{PL} 93%, FWHM 42 nm (20 wt% doped in DBFPO)
λ_{EL} 478 nm Φ_{EL} 30.7%, CIE (0.14, 0.26)
J. Mater. Chem. C **2020**, 8, 2272.

Figure 15. Chemical structures, photophysical properties, and device performance of **3CzTB** and **M3CzB**. Adapted with permission.[59] Copyright 2020, Royal Society of Chemistry.
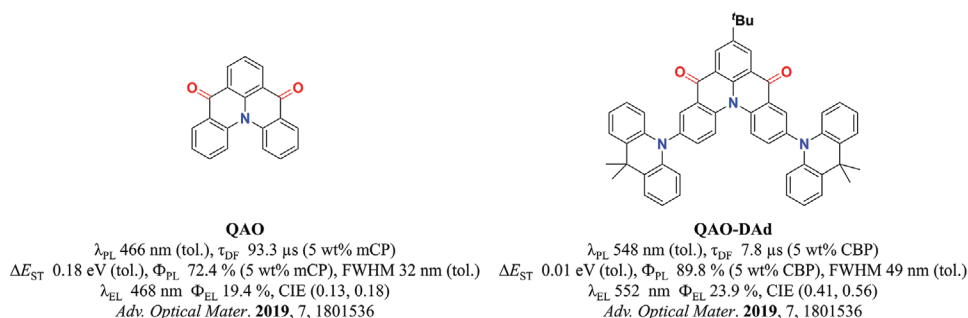
Figure 16. Chemical structures, photophysical properties, and device performances of **QAO** and **QAO-DAd**. Adapted with permission.[60] Copyright 2019, Wiley-VCH.

EQE$_{max}$ (17.8% at 13.5 cd m^{-2}), CE (33.2 cd A^{-1}), PE (34.2 lm W^{-1}) and a high brightness (6785.2 cd m^{-2}) values were noted for this device. Irrespective of the concentration of the compound, all the brominated emitters performed inferior to the other devices, especially the phenothiazine derivatives.

The same group modified the resonant acceptor core **2a** (Figure 2) to generate two new D–A TADF systems with tercarbazole donors (**Figure 15**).[59] In the case of **3CzTB**, acceptor remains the same to their previous report, for the second emitter, **M3CzB**, acceptor is selected without tert-butyl groups at the para positions to oxygen atoms and the pendant carbazoles of the tertcarbazole donor are modified with methyl substituents. From the low temperature PL measurements, the phosphorescence spectra match with that of the corresponding acceptors, showing clearly an LE character. It is surprising that a very minor modification of MR core leads to a 0.09 eV difference in ΔE_{ST} between the two emitters. The emitter (**M3CzB**) with unmodified MR fragment acceptor (**2a**; Figure 2) exhibited ΔE_{ST} of 0.14 eV while for **3CzTB** the ΔE_{ST} is 0.23 eV in toluene. Emission maxima are 433 and 445 nm, respectively, for **3CzTB** and **M3CzB**. Similar to the previous reports, these D–A systems also possess high Φ_{PL}s (88–93%) and short delayed lifetimes (9.3–7.8 μs) in toluene solution. Devices were fabricated in the configuration ITO, 50 nm/HATCN, 7 nm/TAPC, 50 nm/DCDPA, 10 nm/20 wt% dopant in DBFPO, 25 nm/ DBFPO, 5 nm/TPBi, 15 nm/LiF/Al, 1.5/100 nm. The turn-on voltages are around 3 V. The λ_{EL} are redshifted from their corresponding λ_{PL} in toluene solution. The device with **M3CzB** (18 160 cd m^{-2}) was brighter than that with **3CzTB** (11 690 cd m^{-2}) and shows a slightly redshifted emission. The CIE values are (0.14, 0.19) and (0.14, 0.26) respectively for **3CzTB** and **M3CzB**. The corresponding EQE$_{max}$/EQE$_{1000}$/CE$_{max}$/CE$_{1000}$ values are 29.1%/13.5%/36.4 cd A^{-1}/17.1 cd A^{-1} and 30.7%/21.6%/46.7 cd A^{-1}/ 31.4 cd A^{-1} for **3CzTB** and **M3CzB**, respectively. These emitters are also found to be orienting horizontally in the emissive layer, horizontal orientation ratio (θ) = 0.82 and 0.81, respectively for **3CzTB** and **M3CzB** were measured in 20 wt% doped in DBFPO host. The device configuration used for lifetime measurements differed from the previous architecture and was. ITO, 50 nm/HATCN, 7 nm/NPB, 50 nm/PCZAC, 10 nm/20 wt% dopant:mCBP-CN, 25 nm/DDBFT, 5 nm/p-bPPhenB, 15 nm/ LiF, 1.5 nm/Al, 100 nm. Device lifetime measurements evaluated at 400 nits revealed that the device lifetimes (LT$_{50}$) reached 60.5 h and 81 h for **3CzTB** and **M3CzB**-based OLEDs, respectively. Devices fabricated for lifetime measurements exhibited bluer emission than the previous devices fabricated with DBFPO host for efficiency measurements. Compared to the devices with DBFPO host, the device efficiency shown by the devices fabricated for lifetime measurements was significantly lower. The EQE (CIE values) values of these latter devices were 7.6% (0.14, 0.10), and 14.4% (0.13, 0.19) for **3CzTB** and **M3CzB**, respectively.

Another inverted design of the **DABNA** series with the nitrogen atom donor placed centrally was recently reported by Jiang and co-workers[60] The molecule **QOA** consisted of a triphenyl amine having two para-disposed carbonyl bridges (**Figure 16**). This molecule and its derivatives were previously synthesized by Venkataraman and co-workers[53,61] However, their TADF properties were not acknowledged in the original report. In line with previous boron-containing MR-TADF compounds, the PL spectrum of **QAO** was blue (λ_{PL} = 466 nm in toluene), narrow (FWHM = 32 nm), bright (Φ_{PL} = 72.4%, 5 wt% in mCP), and with an associated small ΔE_{ST} of 0.18 eV, properties that are very close to those observed for **DABNA-1** in saturated ethanol (λ_{PL} = 458 nm, FWHM = 36 nm, ΔE_{ST} = 0.15 eV).[27a] Unlike boron-based MR-TADF compounds these ketone-containing molecules are relatively easy to synthesize. Following the previously reported synthesis,[53,61] **QOA** was obtained in a good overall yield of 51%. TD-DFT calculations suggested that the S_0–S_1 transition of QOA has a rather large oscillator strength of 0.157. Time-resolved PL measurements in 5 wt% doped mCP films showed a τ_d of 93.3 μs. The absolute Φ_{PL} of the doped film remained high at 72.4%. Devices were fabricated in a configuration of ITO/HAT-CN, 10 nm/TAPC, 45 nm/TCTA, 10 nm/5 wt% **QAO**:mCP, 20 nm/4,6-Bis(3,5-di(pyridin-4-yl)phenyl)-2-phenylpyrimidine (B3PYMPM),40 nm/8-hydroxyquinolinolato lithium (Liq), 2 nm/Al, 120 nm. The OLED showed a low turn-on voltage of 3 V (1 cd m^{-2}) and a narrow emission (FWHM = 39 nm) band at λ_{EL} = 468 nm, which, though slightly broader, essentially remains very close to the emission in solution. The CIE coordinates were (0.13, 0.18) and the OLED using **QAO** showed poorer color purity than the devices employing boron-based MR-TADF emitters. The device nonetheless exhibited high performance with maximum current efficiency (CE$_{max}$), power efficiency (PE$_{max}$), and EQE$_{max}$ of 26.2 cd A^{-1}, 31.6 lm W^{-1}, and 19.4%, respectively. However, the OLED also suffered from strong efficiency roll-off (56%), which may be due to the long-lived delayed lifetime and deleterious intermolecular interaction from its fused planar structure.
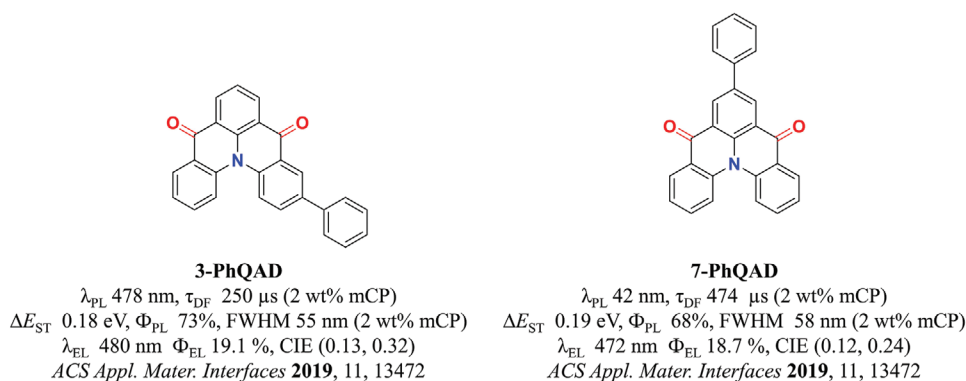
3-PhQAD
λ_{PL} 478 nm, τ_{DF} 250 µs (2 wt% mCP)
ΔE_{ST} 0.18 eV, Φ_{PL} 73%, FWHM 55 nm (2 wt% mCP)
λ_{EL} 480 nm Φ_{EL} 19.1 %, CIE (0.13, 0.32)
ACS Appl. Mater. Interfaces **2019**, 11, 13472

7-PhQAD
λ_{PL} 42 nm, τ_{DF} 474 µs (2 wt% mCP)
ΔE_{ST} 0.19 eV, Φ_{PL} 68%, FWHM 58 nm (2 wt% mCP)
λ_{EL} 472 nm Φ_{EL} 18.7 %, CIE (0.12, 0.24)
ACS Appl. Mater. Interfaces **2019**, 11, 13472

Figure 17. Chemical structures, photophysical properties, and device performances of **3-PhQAD** and **7-PhQAD**. Adapted with permission.[62] Copyright 2019, American Chemical Society.

The same report also used **QAO** core as an acceptor in a conventional donor–acceptor TADF configuration in which DMAc serves as the donor unit (**QAO-DAd**).[60] This structure contains two DMAc donors and a *tert*-butyl substituent located *para* to the central nitrogen atom. DFT calculations predict that the donor is twisted into an orthogonal conformation with respect to the acceptor, leading to well-separated HOMO and LUMO and a correspondingly small ΔE_{ST}. **QAO-DAd** exhibited a high Φ_{PL} of 89.8% in 5 wt% mCP and a very small ΔE_{ST} of 0.01 eV. As with other D–A TADF emitters, **QAO-DAd** exhibited broad emission associated with an ICT transition from the emissive singlet state. Both vacuum-deposited and solution-processed devices were fabricated with this emitter. Vacuum deposited devices were fabricated in the configuration ITO/HAT-CN, 10 nm/ TAPC 45 nm/TCTA, 10 nm/5 wt% **QAO-DAd**:CBP, 20 nm/ TmPyPB, 50 nm/Liq, 2 nm/Al, 120 nm. This device exhibited yellow-green emission with λ_{EL} of 552 nm and CIE coordinates of (0.41, 0.56). The OLED showed excellent performance, with CE_{max}, PE_{max}, and EQE_{max} of 83.3 cd A^{-1}, 75.0 lm W^{-1}, and 23.9%, respectively. In the solution-processed OLED the λ_{EL} was 556 nm. The device performance was somewhat lower but still excellent, especially in the context of solution-processed device [ITO/PEDOT:PSS, 35 nm/5 wt% **QAO-DAd**:CBP (20 nm)/TmPyPB (50 nm)/Liq (2 nm)/Al (120 nm)] performance, with CE_{max}, PE_{max}, and EQE_{max} of 68.2 cd A^{-1}, 51.1 lm W^{-1}, and 19.3% respectively).

Zhang and co-workers reported phenyl-substituted analogs of **QAO**, known as **3-PhQAD** and **7-PhQAD**.[62] These two isomers differ only in the regiochemistry of the phenyl substituent (**Figure 17**). The two isomers were synthesized in an analogous procedure to Jiang and co-workers,[60] with **3-PhQAD** and **7-PhQAD** obtained after chromatographic separation in 53% and 27% yield, respectively. For both emitters, DFT calculations suggest that the additional phenyl ring modulates only to the distribution of the HOMO while the LUMO resides on the fused core. The calculated reorganization energies of 0.22 and 0.08 eV for **3-PhQAD** and **7-PhQAD**, respectively, which showed that **7-PhQAD** would have a narrower emission spectrum compared to **3-PhQAD** isomer. Sharp emission bands and a very small Stokes shifts in toluene solutions were observed, which are hallmarks of MR-TADF emitters. In toluene, both compounds showed narrow, blue emission similar to that of **QOA** core; for **3-PhQAD** (λ_{PL} = 466 nm, FWHM = 30 nm) and **7-PhQAD** (λ_{PL} = 464 nm,

FWHM = 22 nm). There is only a small degree of positive solvatochromism, which the authors contend is evidence of an emissive excited state with mixed LE and CT character (vide infra). The ΔE_{ST} values in 2 wt% mCP film are 0.18 and 0.19 eV for **3-PhQAD** and **7-PhQAD**, respectively, which translated in a long τ_d of 250 and 474 µs, respectively, which is much higher than the parent core (**QOA**) and the DABNA series. The device stack used in this report was ITO/TAPC, 35 nm/TCTA, 10 nm/2 wt% dopant in mCP, 20 nm/TmPyPB, 40 nm/LiF, and 1 nm/Al. The OLEDs with both emitters showed similar efficiencies compared to the device employing the parent **QAO** as the emitter. The **3-PhQAD**-based OLED exhibited a λ_{EL} of 480 nm (FWHM = 44 nm) with CIE coordinates of (0.13, 0.32), while the **7-PhQAD**-based OLED showed a narrower and blueshifted λ_{EL} of 472 nm (FWHM = 34 nm) and CIE coordinates of (0.12, 0.24). The maximum EQE, CE and PE observed for the device with **7-PhQAD** are 18.7%, 28.8 cd A^{-1} and 28.2 lm W^{-1}, similar to the device with **QOA**, while the device with **3-PhQAD** exhibited maximum EQE, CE and PE of 19.1%, 33.5 cd A^{-1} and 32.9 lm W^{-1}. The maximum brightness of the devices that were reached with these emitters are 4975 and 2944 cd m^{-2}, respectively, for **3-PhQAD** and **7-PhQAD** based devices. Both devices, however, suffered from serious efficiency role-off, which was identified to originate from a triplet-triplet annihilation (TTA) channel at low driving voltage based on theoretical stimulations, while at higher driving voltage singlet exciton–polaron annihilation (SPA) and TTA process contributes to the exciton loss channels in the device.

Recently we reported[63] a derivative of **QAO/QAD** (a.k.a. **DiKTa**; Figure 18).[60] Most of the MR-TADF emitters reported involved very low doping, often no more than 1 wt% in film. This was necessary to prevent aggregation-caused quenching (ACQ), which are expectedly large for such planar molecules. In order to mitigate ACQ we developed the mesitylated derivative, **Mes₃DiKTa**. Spin-component scaling second-order approximate Coupled-cluster (SCS-CC2) calculations confirmed that both compounds are MR-TADF, with ΔE_{ST} of 0.27 and 0.26 eV for **DiKTa** and **Mes₃DIKTa**, respectively. The synthetic route of **DiKTa** followed the previously reported protocol.[53,61] Direct bromination of **DiKTa** was not possible, but bromination in high yield of 84% was possible on the diester. Friedel–Crafts acylation produced **Br₃DiKTa**, which was elaborated to install the mesityl groups by Suzuki–Miyaura coupling to afford **Mes₃DiKTa**. Single crystal analysis showed different packing
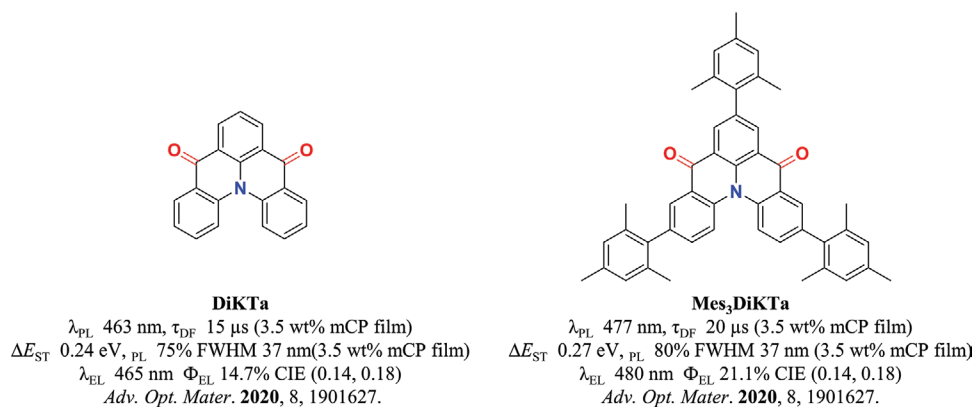
**ADVANCED
SCIENCE NEWS**
www.advancedsciencenews.com

**ADVANCED
FUNCTIONAL
MATERIALS**
www.afm-journal.de

DiKTa
λ_{PL} 463 nm, τ_{DF} 15 μs (3.5 wt% mCP film)
ΔE_{ST} 0.24 eV, $_{PL}$ 75% FWHM 37 nm(3.5 wt% mCP film)
λ_{EL} 465 nm Φ_{EL} 14.7% CIE (0.14, 0.18)
Adv. Opt. Mater. **2020**, 8, 1901627.

Mes₃DiKTa
λ_{PL} 477 nm, τ_{DF} 20 μs (3.5 wt% mCP film)
ΔE_{ST} 0.27 eV, $_{PL}$ 80% FWHM 37 nm (3.5 wt% mCP film)
λ_{EL} 480 nm Φ_{EL} 21.1% CIE (0.14, 0.18)
Adv. Opt. Mater. **2020**, 8, 1901627.

Figure 18. Chemical structures, photophysical properties, and device performances of **DiKTa** and **Mes₃DiKTa**. Adapted with permission.[63] Copyright 2020, Wiley-VCH.

structures with π–π interactions disrupted in the **Mes₃DiKTa** crystal. The modified emitter presented reversible oxidation and reduction waves in the cyclic voltammograms, which is due to the inhibition of electrochemical degradation processes located at the *para* positions to that of central nitrogen. Moderate positive solvatochromism of ≈31 nm for both is observed, consistent with a short-range charge transfer.[49] A modest redshift in the emission from **DiKTa** (453 nm) to **Mes₃DiKTa** (468 nm) in toluene was also noted, which was the result of the inductively electron-withdrawing nature of the mesityl groups that stabilize the LUMO resulting in a reduced band gap. In addition, the modified emitter presented a slightly shorter lifetime of 23 μs in toluene compare to the parent (33 μs). ACQ was strongly suppressed in mCP films of **Mes₃DiKTa**. Further, in neat **DiKTa** films two emission peaks at 475 and 536 nm were observed, the latter of which we attributed to excimer formation. This lower energy emission was not observed in neat films of **Mes₃DiKTa**. In 3.5 wt% emitter in mCP, ΔE_{ST} was calculated to be 0.20 and 0.21 eV for **DiKTa** and **Mes₃DiKTa**, respectively. Devices were fabricated in the configuration ITO/HAT-CN, 10 nm/TAPC, 40 nm/TCTA, 10 nm/3.5 wt% emitter:mCP, 20 nm/TmPyPb, 50 nm/LiF, 1 nm/Al, 100 nm. Both the devise shown a low turn on voltage of 3 V. The OLED with **Mes₃DiKTa** showed an EQE_{max} of 21.2%, (25 cd m^{-2}) which was superior to the device with **DiKTa** at 14.7% (8 cd m^{-2}). Improved efficiency roll-off was observed for the device with

Mes₃DiKTa where there was only 31% roll-off at 100 cd m^{-2} compared to 44% for the OLED with **DiKTa**. Both **DiKTa** and **Mes₃DiKTa** displayed higher brightness than previously reported ketone MR-TADF emitters including that reported with the **QOA** emitter, with maximum luminance values of 10 385 and 12 949 cd m^{-2}, respectively. These luminances compare favorably to that reported for **3-PhQAD** at 4795 cd m^{-2}. Similar to the trends in the solution-state photophysics, a 15 nm redshift in the electroluminescence spectrum was observed for the OLED with **Mes₃DiKTa** to that of **DiKTa**, from CIE (0.14,0.18) to (0.12,0.32).

3. Modeling of MR-TADF Emitters

DFT is the standard computational approach for the investigation of the optoelectronic properties of TADF (and indeed all) emitters. It has been widely, and often wisely, used to rationalize molecular design and provide greater insight into the TADF mechanism. Conventional hybrid functionals, particularly B3LYP,[64] PBE0[65] and range-corrected functionals including omega-tuned LCωPBE[66] have emerged as the most popular in the TADF literature. For D–A TADF emitters, these methods usually offer good quantitative agreement with experiment for both ΔE_{ST} and S_1 energies and qualitative agreement with experiment for spectral linewidths as inferred from calculated

Table 3. Literature-obtained values of TD-DFT calculated and experimentally determined ΔE_{ST} values for all MR-TADF emitters reported to date, and calculations performed by us using SCS-CC2 (excitations are vertical absorption unless stated as adiabatic energy (E_A)).

Compound	Method used in the literature	$\Delta E_{ST(CALC)}$ (E_A) calculated in the literature [eV]	$\Delta E_{ST(EXP)}$ [eV]	$\Delta E_{ST(CALC)}$ SCS[63] [eV]	Ref.
2a	TD-B3LYP/6-31g(d)	N/A (0.52)	0.15	0.20	[28]
DABNA-1	TD-B3LYP/6-31g(d)	0.49 (0.39)	0.18	0.16	[27a]
DABNA-2	TD-B3LYP/6-31g(d)	0.42 (0.30)	0.14	0.14	[27a]
2a	TD-B3LYP/6-311g(d,p)	N/A	0.21	0.17	[33]
TBN-TPA	TD-B3LYP/6-31g	N/A	0.14	0.13	[36]
t-DABNA	N/A	N/A	0.17	0.15	[38]
QAO	TD-B3LYP/6-31g(d)	N/A	0.18	0.27	[60]
3-Ph-QAD	TD-B3LYP/6-31g(d)	0.60	0.18	0.26	[62]
7-Ph-QAD	TD-B3LYP/6-31g(d)	0.55	0.19	0.27	[62]

**ADVANCED
SCIENCE NEWS**
www.advancedsciencenews.com

**ADVANCED
FUNCTIONAL
MATERIALS**
www.afm-journal.de

relaxation energies. Unfortunately, DFT predictions fall apart for MR-TADF emitters, especially in terms of predicted ΔE_{ST} values, often consistently overestimated; notably, and in a way very symptomatic, most reports to date only discuss ground-state DFT calculations, with time-dependent DFT results more rarely presented (**Table 3**). In order to tackle the modeling of this class of emitters, several theory papers have emerged. The excited-state dynamics of **DABNA-1** and **DABNA-2** were investigated[67] to rationalize why **DABNA-2** shows an enhanced Φ_{PL} in the film compared to solution, while for **DABNA-1** there is little change in the Φ_{PL}.[27a] Differing nonradiative decay processes were proposed for the two emitters.[67] In **DABNA-2** nonradiative decay is dominated by low frequency twisting of the pendant phenyl groups, which would be significantly suppressed in the solid state. In **DABNA-1** the C–C stretching is the primary source of nonradiative decay. As these stretching modes are high-frequency processes there would be no significant difference between solution and film. Large ΔE_{ST} values of 0.33 eV were predicted for both compounds, which significantly overestimate the experimentally determined values; DFT calculations do predict the presence of two intermediate triplet states sandwiched between T_1 and S_1. Although the authors contend that ISC takes place mainly between S_1 and T_2 due to their strongly coupled nature, the primary route for RISC was proposed to be T_1 to S_1. This proposed mechanism differs from the one postulated by Northey and Penfold,[67b] who propose that T_2 to S_1 is the primary route of RISC for **DABNA-1**, with almost no contribution from T_1. Quantum dynamics calculations of the T_1 and T_2 populations were applied to justify this mechanism, and k_{RISC} was compared to experimentally derived values. There was poor agreement when considering only 1 singlet state within the model; however, when higher-lying singlet states were incorporated, the predictions became more accurate. The coupling between S_1 and higher energy singlet states helped improve spin–orbit coupling, which was mediated via vibronic coupling occurring within the molecule. Because RISC is facilitated by vibronic coupling between singlet states, the rigid nature of this emitter implies a slower k_{RISC} than exists in conventional D–A TADF emitters, which have more conformational freedom. Although the modeling does accurately model the RISC kinetics, again ΔE_{ST} was poorly predicted, with a value of 0.59 eV being reported.[67b] When the functional MPWK1CIS was used to model **DABNA-1** and **DABNA-2**, good agreement between $\Delta E_{ST(EXP)}$ (0.18 eV) and $\Delta E_{ST(CALC)}$ (0.21 eV) was obtained.[68] No explanation was provided as to why this approach worked so well. This methodology was used to predict ΔE_{ST} and k_f for both **DABNA-1** and **DABNA-2**, and for a series of functionalized derivatives incorporating additional donor moieties to the **DABNA-1** core.

We recently reported a much-improved computational protocol to model MR-TADF compounds, moving away from DFT and using instead a wave function-based approach, SCS-CC2.[49] Excellent agreement was achieved for the ΔE_{ST} values of both **DABNA-1** and **2a** (Figure 4) and a proposed design of new extended derivatives offered a tantalizing path to generate molecules showing both decreasing ΔE_{ST} and increasing oscillator strength. The success of this method is ascribed to the inclusion of second-order contributions to the excitations energy that include to some extent double excitations which offer in comparison to TD-DFT a better treatment of both the dynamic and the static electron correlation leading to a better estimate of the S_1 energy. Overall, the poor description in TD-DFT with the conventional functional (hybrid and range-separated) of the S_1 excited state inherently results in an overestimated ΔE_{ST} for the MR-TADF emitters (**Figure 19**).[49,63] This work also offered a design strategy to simultaneously reduce ΔE_{ST} and increase oscillator strength, which is not possible for D–A TADF emitters (Figure 19d). Extension of the DABNA core produced compounds that had reduced ΔE_{ST}, from 0.17 eV in **3** to 0.003 eV in **6**, accompanied by increased oscillator strength for the S_0–S_1 transition from 0.23 to 1.07; increasing the conjugation in these DABNA derivatives also resulted in a predicted redshift in the emission due to the increase in excited state wavefunction delocalization. Further tuning of the emission wavelength can be achieved, for instance by introducing additional N- or B-atoms into the compound. For the sake of illustration, we designed two other molecules, **7** and **8**, based on **5**. These chromophores essentially retain the properties of the parent molecule in terms of ΔE_{ST} and oscillator strength but with tuned emission, blueshifted to 2.85 eV (435 nm, deep blue, **7**) and redshifted to 2.1 eV (590 nm, yellow, **8**) compared to **5**. Up to now, color tuning has proved difficult with the current cohort of MR-TADF emitters covering only 100 nm range, spanning deep blue to sky blue. Although the prospect of efficient blue devices is desirable, the concept of a rigid TADF red emitter mitigating k_{nr} is underexplored yet seemingly possible with our design.

4. Conclusions and Outlook

OLEDs using purely organic D–A TADF compounds have achieved comparable, and for some colors even surpassed, performance metrics compared to state-of-the-art OLEDs employing organometallic phosphorescent complexes.[17] Color purity remains an issue, particularly for blue-emitting devices, and this can best be addressed with narrow-band emitters. MR-TADF emitters in this regard distinguish themselves from D–A TADF emitters, and provide a potential, and long-sought after, solution for high efficiency pure blue OLEDs. Efficiency roll-off remains an issue to be adequately addressed for MR-TADF-based OLEDs, with poor roll-off for most emitters, and device stability is yet to be optimized. However, despite the small number of structurally related examples reported, it is already evident that MR-TADF emitters are an incredibly promising class of compounds. Especially through the report of **ν-DABNA** from Hatakeyama and co-workers,[29b] MR-TADF compounds have set high standards as pure blue TADF emitters. The device with **ν-DABNA** exhibited pure blue emission (CIE = 0.12, 0.11) due in part to its very narrow emission band (FWHM = 18 nm) and showed a remarkable EQE_{max} of 34.4%, which fell only to 26% at 1000 cd m^{-2}. The FWHM of this device is the same as that of the best micro LED device[69] and smaller than that reported from a high-performance QD-LED device.[70] It remains to be seen whether high-performance MR-TADF emitters can be developed in the pure green and red regions of the visible spectrum. Devices reported by Duan and co-workers[48] demonstrated an impressive CIE_y of 0.60, indicates the potential of MR-TADF emitters to address colors other than blue in
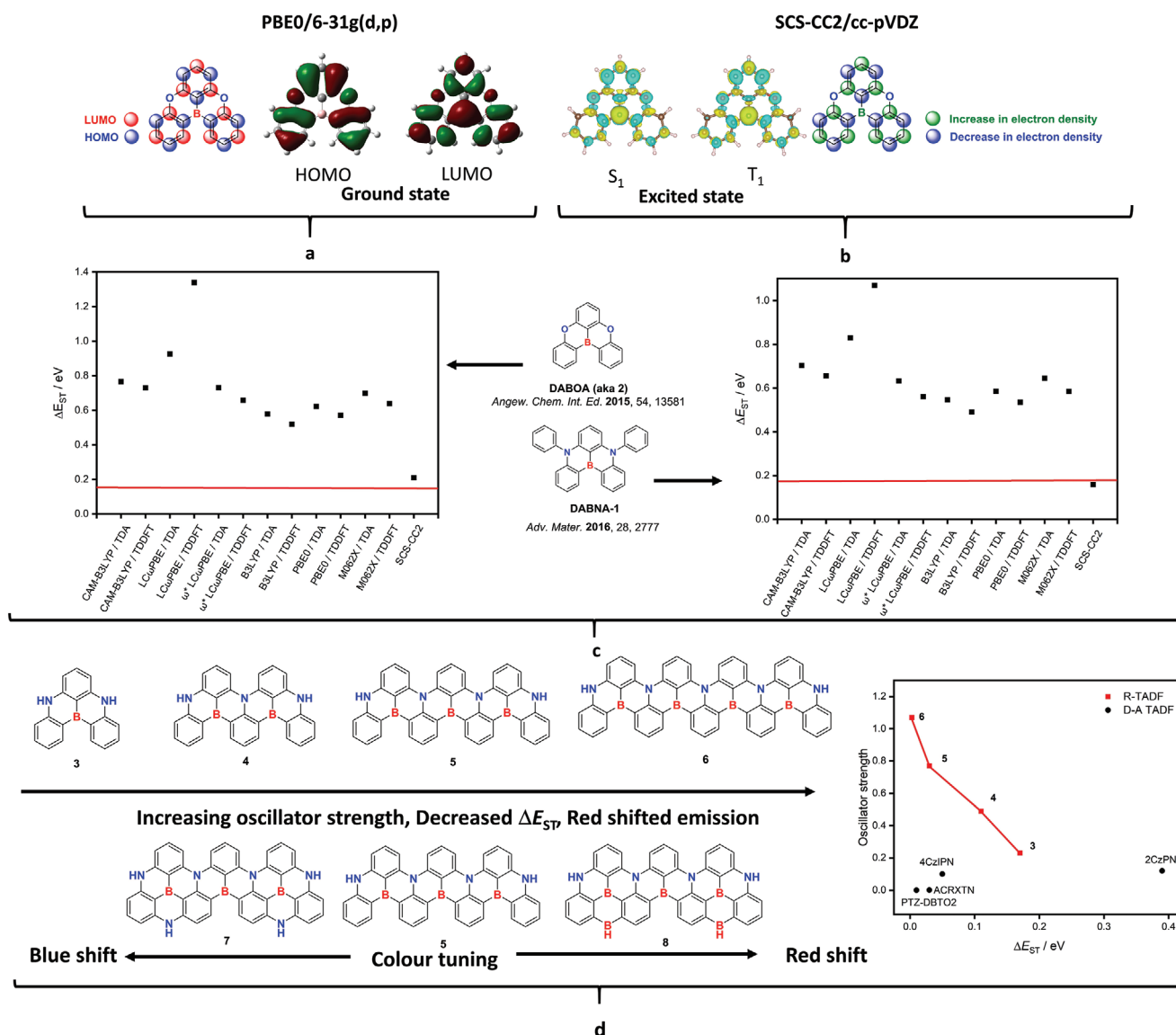
Figure 19. a) Orbital contour plots of the HOMO and LUMO orbitals. b) Difference density plots between the S_0–S_1 and S_0–T_1 transitions of **2a**. c) Predicted ΔE_{ST} using established hybrid, range separated functionals, and SCS–CC2 compared to experimental (red line) for two literature emitters, adapted from our previous work.[63] Reproduced under the terms and conditions of the Creative Commons Attribution license CC BY.[63] Copyright 2019, The Authors, published by Wiley-VCH. d) Evolution of the oscillator strength as a function of ΔE_{ST} for DABNA and the designed compounds **4** to **6**, adapted from our previous report.[49] Color tuning of structure **5** with proposed emitters **7** and **8**. Reproduced under the terms and conditions of the Creative Commons Attribution license CC BY.[49] Copyright 2019, The Authors, published by Springer Nature.

OLEDs. A more complete understanding of the design rules for developing MR-TADF emitters is required, as is an exploration of a wider chemical space beyond triangulene-type compounds. Most of the MR-TADF emitters are reported to have very small delayed contributions to the radiative decay process, which is likely the result of the moderate ΔE_{ST} values that though sufficiently small to turn on TADF nevertheless govern an inefficient RISC process. On a more fundamental level, additional study is required to strengthen an understanding of the excited-state behavior of this class of compounds, including how to modulate emission color, ΔE_{ST} and k_{rISC}. The importance of intermediate triplet states, identified as important in efficient D–A TADF emitters, has not been systematically considered in MR-TADF

compounds. Finally, it is only recently that an adequate computational model has been developed. With this in hand in silico design of new MR-TADF emitters becomes feasible, which should lead to an acceleration of materials discovery.

Acknowledgements

Conflict of Interest

The authors declare no conflict of interest.

Keywords

[1] R. Delorme, F. Perrin, *J. Phys. Radium* **1929**, *10*, 177.

[2] G. N. Lewis, D. Lipkin, T. T. Magel, *J. Am. Chem. Soc.* **1941**, *63*, 3005.

[3] a) C. A. Parker, T. A. Joyce, *Photochem. Photobiol.* **1967**, *6*, 395; b) C. A. Parker, C. G. Hatchard, *Trans. Faraday Soc.* **1961**, *57*, 1894.

[4] M. N. Berberan-Santos, J. M. M. Garcia, *J. Am. Chem. Soc.* **1996**, *118*, 9391.

[5] R. E. Brown, L. A. Singer, J. H. Parks, *Chem. Phys. Lett.* **1972**, *14*, 193.

[6] a) A. Maciejewski, M. Szymanski, R. P. Steer, *J. Phys. Chem.* **1986**, *90*, 6314; b) M. Szymanski, A. Maciejewski, R. P. Steer, *J. Phys. Chem.* **1988**, *92*, 2485.

[7] M. Sikorski, I. V. Khmelinskii, W. Augustyniak, F. Wilkinson, *J. Chem. Soc., Faraday Trans.* **1996**, *92*, 3487.

[8] B. S. Yamanashi, D. M. Hercules, *Appl. Spectrosc.* **1971**, *25*, 457.

[9] A. Endo, M. Ogasawara, A. Takahashi, D. Yokoyama, Y. Kato, C. Adachi, *Adv. Mater.* **2009**, *21*, 4802.

[10] J. C. Deaton, S. C. Switalski, D. Y. Kondakov, R. H. Young, T. D. Pawlik, D. J. Giesen, S. B. Harkins, A. J. M. Miller, S. F. Mickenberg, J. C. Peters, *J. Am. Chem. Soc.* **2010**, *132*, 9499.

[11] a) R. Czerwieniec, K. Kowalski, H. Yersin, *Dalton Trans.* **2013**, *42*, 9826; b) M. J. Leitl, F.-R. Küchle, H. A. Mayer, L. Wesemann, H. Yersin, *J. Phys. Chem. A* **2013**, *117*, 11823; c) M. J. Leitl, V. A. Krylova, P. I. Djurovich, M. E. Thompson, H. Yersin, *J. Am. Chem. Soc.* **2014**, *136*, 16032; d) C. L. Linfoot, M. J. Leitl, P. Richardson, A. F. Rausch, O. Chepelin, F. J. White, H. Yersin, N. Robertson, *Inorg. Chem.* **2014**, *53*, 10854; e) T. Hofbeck, U. Monkowius, H. Yersin, *J. Am. Chem. Soc.* **2015**, *137*, 399.

[12] a) V. A. Krylova, P. I. Djurovich, B. L. Conley, R. Haiges, M. T. Whited, T. J. Williams, M. E. Thompson, *Chem. Commun.* **2014**, *50*, 7176; b) R. Hamze, J. L. Peltier, D. Sylvinson, M. Jung, J. Cardenas, R. Haiges, M. Soleilhavoup, R. Jazzar, P. I. Djurovich, G. Bertrand, M. E. Thompson, *Science* **2019**, *363*, 601.

[13] a) D. M. Zink, D. Volz, T. Baumann, M. Mydlak, H. Flügge, J. Friedrichs, M. Nieger, S. Bräse, *Chem. Mater.* **2013**, *25*, 4471; b) M. Wallesch, D. Volz, D. M. Zink, U. Schepers, M. Nieger, T. Baumann, S. Bräse, *Chem. – Eur. J.* **2014**, *20*, 6578.

[14] a) C. Bizzarri, C. Strabler, J. Prock, B. Trettenbrein, M. Ruggenthaler, C.-H. Yang, F. Polo, A. Iordache, P. Brüggeller, L. D. Cola, *Inorg. Chem.* **2014**, *53*, 10944; b) D. Liang, X.-L. Chen, J.-Z. Liao, J.-Y. Hu, J.-H. Jia, C.-Z. Lu, *Inorg. Chem.* **2016**, *55*, 7467; c) Z. Wang, C. Zheng, W. Wang, C. Xu, B. Ji, X. Zhang, *Inorg. Chem.* **2016**, *55*, 2157; d) F. Dumur, *Org. Electron.* **2015**, *21*, 27.

[15] A. Endo, K. Sato, K. Yoshimura, T. Kai, A. Kawada, H. Miyazaki, C. Adachi, *Appl. Phys. Lett.* **2011**, *98*, 083302.

[16] H. Uoyama, K. Goushi, K. Shizu, H. Nomura, C. Adachi, *Nature* **2012**, *492*, 234.

[17] M. Y. Wong, E. Zysman-Colman, *Adv. Mater.* **2017**, *29*, 1605444.

[18] a) K. Hanaoka, K. Kikuchi, S. Kobayashi, T. Nagano, *J. Am. Chem. Soc.* **2007**, *129*, 13502; b) S. Nagl, C. Baleizão, S. M. Borisov, M. Schäferling, M. N. Berberan-Santos, O. S. Wolfbeis, *Angew. Chem., Int. Ed.* **2007**, *46*, 2317.

[19] A. Al Mousawi, D. M. Lara, G. Noirbent, F. Dumur, J. Toufaily, T. Hamieh, T.-T. Bui, F. Goubard, B. Graff, D. Gigmes, J. P. Fouassier, J. Lalevée, *Macromolecules* **2017**, *50*, 4913.

[20] R. Ishimatsu, S. Matsunami, T. Kasahara, J. Mizuno, T. Edura, C. Adachi, K. Nakano, T. Imato, *Angew. Chem., Int. Ed.* **2014**, *53*, 6993.

[21] H. Nakanotani, T. Furukawa, T. Hosokai, T. Hatakeyama, C. Adachi, *Adv. Opt. Mater.* **2017**, *5*, 1700051.

[22] Q. Zhang, S. Xu, M. Li, Y. Wang, N. Zhang, Y. Guan, M. Chen, C.-F. Chen, H.-Y. Hu, *Chem. Commun.* **2019**, *55*, 5639.

[23] M. Segal, M. A. Baldo, R. J. Holmes, S. R. Forrest, Z. G. Soos, *Phys. Rev. B* **2003**, *68*, 075211.

[24] M. A. El-Sayed, *J. Chem. Phys.* **1963**, *38*, 2834.

[25] P. K. Samanta, D. Kim, V. Coropceanu, J.-L. Brédas, *J. Am. Chem. Soc.* **2017**, *139*, 4042.

[26] C. Adachi, *Jpn. J. Appl. Phys.* **2014**, *53*, 060101.

[27] a) T. Hatakeyama, K. Shiren, K. Nakajima, S. Nomura, S. Nakatsuka, K. Kinoshita, J. Ni, Y. Ono, T. Ikuta, *Adv. Mater.* **2016**, *28*, 2777; b) C. Deng, Y. Niu, Q. Peng, A. Qin, Z. Shuai, B. Z. Tang, *J. Chem. Phys.* **2011**, *135*, 014304.

[28] H. Hirai, K. Nakajima, S. Nakatsuka, K. Shiren, J. Ni, S. Nomura, T. Ikuta, T. Hatakeyama, *Angew. Chem., Int. Ed.* **2015**, *54*, 13581.

[29] a) K. Matsui, S. Oda, K. Yoshiura, K. Nakajima, N. Yasuda, T. Hatakeyama, *J. Am. Chem. Soc.* **2018**, *140*, 1195; b) Y. Kondo, K. Yoshiura, S. Kitera, H. Nishi, S. Oda, H. Gotoh, Y. Sasada, M. Yanai, T. Hatakeyama, *Nat. Photonics* **2019**, *13*, 678.

[30] Z. Yang, Z. Mao, Z. Xie, Y. Zhang, S. Liu, J. Zhao, J. Xu, Z. Chi, M. P. Aldred, *Chem. Soc. Rev.* **2017**, *46*, 915.

[31] a) K.-C. Wu, P.-J. Ku, C.-S. Lin, H.-T. Shih, F.-I. Wu, M.-J. Huang, J.-J. Lin, I.-C. Chen, C.-H. Cheng, *Adv. Funct. Mater.* **2008**, *18*, 67; b) S. J. Lee, J. S. Park, K.-J. Yoon, Y.-I. Kim, S.-H. Jin, S. K. Kang, Y.-S. Gal, S. Kang, J. Y. Lee, J.-W. Kang, S.-H. Lee, H.-D. Park, J.-J. Kim, *Adv. Funct. Mater.* **2008**, *18*, 3922; c) J.-Y. Hu, Y.-J. Pu, F. Satoh, S. Kawata, H. Katagiri, H. Sasabe, J. Kido, *Adv. Funct. Mater.* **2014**, *24*, 2064; d) S. Zhang, L. Yao, Q. Peng, W. Li, Y. Pan, R. Xiao, Y. Gao, C. Gu, Z. Wang, P. Lu, F. Li, S. Su, B. Yang, Y. Ma, *Adv. Funct. Mater.* **2015**, *25*, 1755.

[32] H. Nakanotani, T. Furukawa, C. Adachi, *Adv. Opt. Mater.* **2015**, *3*, 1381.

[33] S. Nakatsuka, H. Gotoh, K. Kinoshita, N. Yasuda, T. Hatakeyama, *Angew. Chem., Int. Ed.* **2017**, *56*, 5087.

[34] F. Miyamoto, S. Nakatsuka, K. Yamada, K.-I. Nakayama, T. Hatakeyama, *Org. Lett.* **2015**, *17*, 6158.

[35] Y. Kitamoto, T. Suzuki, Y. Miyata, H. Kita, K. Funaki, S. Oi, *Chem. Commun.* **2016**, *52*, 7098.

[36] X. Liang, Z.-P. Yan, H.-B. Han, Z.-G. Wu, Y.-X. Zheng, H. Meng, J.-L. Zuo, W. Huang, *Angew. Chem., Int. Ed.* **2018**, *57*, 11316.

[37] H.-B. Han, X.-F. Ma, Z.-G. Wu, Y.-X. Zheng, *Mater. Chem. Front.* **2018**, *2*, 1284.

[38] S. H. Han, J. H. Jeong, J. W. Yoo, J. Y. Lee, *J. Mater. Chem. C* **2019**, *7*, 3082.

[39] Q. Zhang, B. Li, S. Huang, H. Nomura, H. Tanaka, C. Adachi, *Nat. Photonics* **2014**, *8*, 326.

[40] a) K. H. Lee, J. Y. Lee, H. Y. Oh, *SID Symp. Dig. Tech. Pap.* **2019**, *50*, 1924; b) K. H. Lee, J. Y. Lee, *Org. Electron.* **2019**, *75*, 105377.

[41] K. H. Lee, J. Y. Lee, *J. Mater. Chem. C* **2019**, *7*, 8562.

[42] S. H. Han, J. Y. Lee, *J. Mater. Chem. C* **2018**, *6*, 1504.

[43] Y. Kwon, S. H. Han, S. Yu, J. Y. Lee, K. M. Lee, *J. Mater. Chem. C* **2018**, *6*, 4565.

[44] A. Maheshwaran, V. G. Sree, H.-Y. Park, H. Kim, S. H. Han, J. Y. Lee, S.-H. Jin, *Adv. Funct. Mater.* **2018**, *28*, 1802945.

[45] a) K. Masui, H. Nakanotani, C. Adachi, *Org. Electron.* **2013**, *14*, 2721; b) D. L. Crossley, I. Vitorica-Yrezabal, M. J. Humphries, M. L. Turner, M. J. Ingleson, *Chem. – Eur. J.* **2016**, *22*, 12439.

[46] M. K. Etherington, J. Gibson, H. F. Higginbotham, T. J. Penfold, A. P. Monkman, *Nat. Commun.* **2016**, *7*, 13680.

[47] T. B. Nguyen, H. Nakanotani, T. Hatakeyama, C. Adachi, *Adv. Mater.* **2020**, *32*, 1906614.

[48] Y. Zhang, D. Zhang, J. Wei, Z. Liu, Y. Lu, L. Duan, *Angew. Chem., Int. Ed.* **2019**, *58*, 16912.

[49] A. Pershin, D. Hall, V. Lemaur, J.-C. Sancho-Garcia, L. Muccioli, E. Zysman-Colman, D. Beljonne, Y. Olivier, *Nat. Commun.* **2019**, *10*, 597.

[50] S. M. Suresh, E. Duda, D. Hall, Z. Yao, S. Bagnich, A. M. Z. Slawin, D. Beljonne, H. Bässler, D. Beljonne, M. Buck, Y. Olivier, A. Köhler, E. Zysman-Colman, *J. Am. Chem. Soc.* **2020**, *142*, 6588.

[51] T. Agou, J. Kobayashi, T. Kawashima, *Org. Lett.* **2006**, *8*, 2241.

[52] F. B. Dias, J. Santos, D. R. Graves, P. Data, R. S. Nobuyasu, M. A. Fox, A. S. Batsanov, T. Palmeira, M. N. Berberan-Santos, M. R. Bryce, A. P. Monkman, *Adv. Sci.* **2016**, *3*, 1600080.

[53] J. E. Field, T. J. Hill, D. Venkataraman, *J. Org. Chem.* **2003**, *68*, 6071.

[54] S. Oda, B. Kawakami, R. Kawasumi, R. Okita, T. Hatakeyama, *Org. Lett.* **2019**, *21*, 9311.

[55] J. A. Knöller, G. Meng, X. Wang, D. Hall, A. Pershin, D. Beljonne, Y. Olivier, S. Laschat, E. Zysman-Colman, S. Wang, *Angew. Chem., Int. Ed.* **2020**, *59*, 3156.

[56] G. Meng, X. Chen, X. Wang, N. Wang, T. Peng, S. Wang, *Adv. Opt. Mater.* **2019**, *7*, 1900130.

[57] D. H. Ahn, S. W. Kim, H. Lee, I. J. Ko, D. Karthik, J. Y. Lee, J. H. Kwon, *Nat. Photonics* **2019**, *13*, 540.

[58] D. Song, Y. Yu, L. Yue, D. Zhong, Y. Zhang, X. Yang, Y. Sun, G. Zhou, Z. Wu, *J. Mater. Chem. C* **2019**, *7*, 11953.

[59] D. Karthik, D. H. Ahn, J. H. Ryu, H. Lee, J. H. Maeng, J. Y. Lee, J. H. Kwon, *J. Mater. Chem. C* **2020**, *8*, 2272.

[60] Y. Yuan, X. Tang, X.-Y. Du, Y. Hu, Y.-J. Yu, Z.-Q. Jiang, L.-S. Liao, S.-T. Lee, *Adv. Opt. Mater.* **2019**, *7*, 1801536.

[61] J. E. Field, D. Venkataraman, *Chem. Mater.* **2002**, *14*, 962.

[62] X. Li, Y.-Z. Shi, K. Wang, M. Zhang, C.-J. Zheng, D.-M. Sun, G.-L. Dai, X.-C. Fan, D.-Q. Wang, W. Liu, Y.-Q. Li, J. Yu, X.-M. Ou, C. Adachi, X.-H. Zhang, *ACS Appl. Mater. Interfaces* **2019**, *11*, 13472.

[63] D. Hall, S. M. Suresh, P. L. dos Santos, E. Duda, S. Bagnich, A. Pershin, P. Rajamalli, D. B. Cordes, A. M. Z. Slawin, D. Beljonne, A. Köhler, I. D. W. Samuel, Y. Olivier, E. Zysman-Colman, *Adv. Opt. Mater.* **2020**, *8*, 1901627.

[64] Y. Olivier, J. C. Sancho-Garcia, L. Muccioli, G. D'Avino, D. Beljonne, *J. Phys. Chem. Lett.* **2018**, *9*, 6149.

[65] M. Moral, L. Muccioli, W. J. Son, Y. Olivier, J. C. Sancho-García, *J. Chem. Theory Comput.* **2015**, *11*, 168.

[66] H. Sun, C. Zhong, J.-L. Brédas, *J. Chem. Theory Comput.* **2015**, *11*, 3851.

[67] a) L. Lin, J. Fan, L. Cai, C.-K. Wang, *Mol. Phys.* **2018**, *116*, 19; b) T. Northey, T. J. Penfold, *Org. Electron.* **2018**, *59*, 45.

[68] Y. Gao, Q.-Q. Pan, L. Zhao, Y. Geng, T. Su, T. Gao, Z.-M. Su, *Chem. Phys. Lett.* **2018**, *701*, 98.

[69] K. Zhang, D. Peng, K. M. Lau, Z. Liu, *J. Soc. Inf. Disp.* **2017**, *25*, 240.

[70] Y. Yang, Y. Zheng, W. Cao, A. Titov, J. Hyvonen, J. R. Manders, J. Xue, P. H. Holloway, L. Qian, *Nat. Photonics* **2015**, *9*, 259.